Materials Horizons

ROYAL SOCIETY OF CHEMISTRY

REVIEW

View Article Online
View Journal | View Issue

Cite this: *Mater. Horiz.*, 2022, 9, 2473

Lamination methods for the fabrication of perovskite and organic photovoltaics

Aliakbar Ghaffari,[ab] Zahra Saki,[*b] Nima Taghavinia,[bc] Mahdi Malekshahi Byranvand[*de] and Michael Saliba[*de]

Received 30th May 2022,
Accepted 18th July 2022

DOI: 10.1039/d2mh00671e

rsc.li/materials-horizons

Perovskite solar cells (PSCs) have shown rapid progress in a decade of extensive research and development, aiming now towards commercialization. However, the development of more facile, reliable, and reproducible manufacturing techniques will be essential for industrial production. Many lamination methods have been initially designed for organic photovoltaics (OPVs), which are conceptually similar to PSCs. Lamination could provide a low-cost and adaptable technique for the roll-to-roll production of solar cells. This review presents an overview of lamination methods for the fabrication of PSCs and OPVs. The lamination of different electrodes consisting of various materials such as metal back contacts, photoactive layers, hole transport layers (HTLs), and electron transport layers (ETLs) is discussed. The efficiency and stability of the laminated devices are also presented. Finally, the challenges and opportunities of laminated solar cells are discussed.

1. Introduction

Extensive research on photovoltaic (PV) technologies has led to new low-cost, high-performance third-generation solar cells such as dye-sensitized solar cells (DSSCs),[1–6] quantum-dot solar cells (QDSCs),[7] organic photovoltaics (OPVs),[8–10] and perovskite solar cells (PSCs).[11–18] However, most of these emerging technologies are still in the research phase and require more developments to reach commercial applications.[19,20] Among third-generation solar cells, PSCs and OPVs could be turned into printable technologies as they have reached a suitable

[a] *School of Chemistry, College of Science, University of Tehran, 14155 Tehran, Iran*
[b] *Department of Physics, Sharif University of Technology, 14588 Tehran, Iran. E-mail: zahra.saki@sharif.edu*
[c] *Institute for Nanoscience and Nanotechnology, Sharif University of Technology, 14588 Tehran, Iran*
[d] *Institute for Photovoltaics (ipv), University of Stuttgart, Pfafenwaldring 47, 70569 Stuttgart, Germany. E-mail: mahdi.malekshahi@ipv.uni-stuttgart.de, michael.saliba@ipv.uni-stuttgart.de*
[e] *Helmholtz Young Investigator Group FRONTRUNNER, IEK5-Photovoltaik, Forschungszentrum Jülich, 52425 Jülich, Germany*

Aliakbar Ghaffari

Aliakbar Ghaffari received his BSc and MSc degrees in Applied Chemistry from Guilan University and University of Tehran, Iran, in 2015 and 2017, respectively. Since then, he has collaborated with other researchers in the field of polymer chemistry and renewable energies. Currently, he is a member of the Nanoparticles and Coatings Lab (NCL) at the Physics department, Sharif University of Technology. His research interests are materials chemistry, thin-film optoelectronic devices, and perovskite solar cells.

Zahra Saki

Zahra Saki is currently a postdoctoral researcher at Sharif University of Technology (SUT), Iran, from where she obtained her PhD degree in Physics in 2019, focusing on inverted perovskite solar cells. One year of her PhD work was carried out at Uppsala University in Sweden in the group of Prof. Gerrit Boschloo. She was awarded as outstanding PhD candidate from National Elite Foundation of Iran in 2015. Her research interests concentrate on device engineering, perovskite passivation, and perovskite crystallization for perovskite solar cells in the group of Prof. Nima Taghavinia.

power conversion efficiency (PCE) and stability.[21–23] The PCE of PSCs has increased from 3.8% in 2009[24] to 25.7% in 2022,[25,26] and in case of OPVs, it has developed from 2.5% in 2000[27] to 18.2% in 2022.[28,29]

Generally, PSCs are composed of the transparent conductive electrode (TCE) and/or transparent conductive oxide (TCO) glass substrate, the electron transporting layer (ETL), perovskite film as the light absorber, the hole transporting layer (HTL), and the metal back contact.[30–34] In the case of OPVs, the conventional structure includes the TCE glass substrate, HTL, light absorber consisting of a bilayer or mixture of p-type (an electron acceptor) and n-type materials (an electron donor), the buffer layer, and metal back contact.[35,36] The ease of device fabrication for both PSCs and OPVs utilizing solution-processed methods such as spin-coating, slot-die coating, or inkjet printing is the key factor in their success.[14,37–39] However, the deposition of a metal back contact in both kinds of solar cells is the most challenging part of device fabrication, which mainly needs a vacuum-based processing such as thermal evaporation or physical vapor deposition (PVD).[40–43] Unfortunately, the metal can diffuse into the uncompleted solar cell, *i.e.*, photoactive/HTL or ETL films, during these processes; this leads to shunting within the devices and thus performance losses.[44] In addition, using expensive metals such as gold or silver could hamper commercialization.[45,46] For example, although silver is cheaper than gold, unfortunately, it undergoes corrosion reactions with the photoactive layer and facilitates device degradation.[47] Therefore, substituting the noble metal back contacts with inexpensive and inert materials is an important direction to decrease fabrication costs and improve device stability.[14,48] In this regard, low-cost carbon materials with low reactivity have been introduced as promising candidates for this purpose in both PSCs and OPVs.[49–52]

Furthermore, lamination methods have been introduced as a low-cost alternative approach for stacking the pre-deposited metal back contact electrode onto photoanode electrodes in PSCs.[53] Besides, laminated PSCs render the merits of self-encapsulation and stability enhancement. Moreover, this method possesses high operational capability through the parallel preparation of the top and bottom layers, adopting the conventional layer-by-layer deposition methods.[54–57] Initially, the lamination method was used to implement carbon nanotubes (CNTs) as a bifunctional hole transporter and back contact layer onto the PSC configuration.[58] For a favored back contact in PSC architecture, one should consider the energy/Fermi levels alignment, work function in the −4.1 to −5.1 eV

Nima Taghavinia

Nima Taghavinia received his BSc and MSc degrees in Physics from Sharif University of Technology, Iran, in 1994 and 1996, respectively. He received his PhD in Materials Science from Tohoku University, Japan, in 2002. Since then, he has been a faculty member of the Physics department and a member of Institute for Nanoscience and Nanotechnology at Sharif University of Technology. His group conducts research on printable perovskite solar cells.

Mahdi Malekshahi Byranvand

Mahdi Malekshahi Byranvand is a researcher at the Forschungszentrum Jülich and Institute for Photovoltaics (ipv) at the University of Stuttgart. Previously, he worked on different parts of perovskite solar cells during his postdoctoral fellowships at Karlsruhe Institute of Technology (KIT), Pohang University of Science and Technology (POSTECH), and Sharif University of technology. He received his PhD in Inorganic Chemistry from the University of Tehran in 2015, working on photon management in dye-sensitized solar cells. His research interests are currently focused on all-inorganic perovskites, large-scale deposition, passivation of perovskite films, and perovskite tandem solar cells in Prof. Michael Saliba's group.

Michael Saliba

Michael Saliba is the Director of the Institute for Photovoltaics (ipv) at the University of Stuttgart with a dual appointment as the Helmholtz Young Investigator at the Forschungszentrum Jülich, Germany. His research focuses on a deeper fundamental understanding and improvement of optoelectronic properties of emerging photovoltaic materials with an emphasis on perovskites for a sustainable energy future. Previously, he held positions at TU Darmstadt, University of Fribourg, and EPFL. He obtained his PhD from Oxford University. Among others, he received the Heinz-Maier-Leibnitz Award of the German Research Foundation, and was named as one of the 35 innovators worldwide under 35 by MIT Technology Review. Since 2021, he is the Speaker of the DFG Graduate School (GRK) 2642 for "Quantum Engineering". In 2022, he was awarded a Starting Grant by the European Research Council (ERC).

range, electrical conductivity, and stability of the fabricated electrodes. Later, this method was applied for different parts of device architectures, including stacking the perovskite/perovskite interface on separate substrates,[54,59] or wet pre-deposited HTL/perovskite interface, *i.e.*, sandwich structure.[56,57,60] The hot-pressing of the transparent conductive adhesive (TCA) to stick the top electrode into the pre-fabricated ETL/perovskite/HTL stack was also adopted as a premier lamination method.[61,62] Moreover, the mechanical lamination of two half-stacks using a vacuum hot embossing machine[63,64] or a double clip[65] was performed to fabricate both rigid and flexible PSCs. However, one of the most dominant challenges in using this method for PSC fabrication is the sensitivity of organic–inorganic perovskite films to high temperatures and pressures due to the volatile components and the soft nature of perovskite films.[66–69]

The lamination methods also have been used for stacking different parts of the OPV devices, including polymeric top electrodes using an adhesive,[70–72] the photoactive polymer layer,[73,74] or anode and cathode half stacks.[75,76] Likewise, laminated-OPVs employ similar strategies as laminated-PSCs regarding the substrate, equipment, and processes.[71,77–79] Notwithstanding, the main differences between lamination methods in PSCs and OPVs are in the involved materials, solution options, and drying steps due to the sensitivity of perovskite films to polar solvents.

This review focuses on stacking different layers *via* various lamination methods to fabricate highly efficient and stable solar cells. The lamination of numerous layers such as poly(3,4-ethylenedioxitiophene):poly(styrene sulfonate) (PEDOT:PSS), carbon materials, and metals as top or bottom contacts for fabricating PSCs or OPVs are discussed. The advantages and challenges of each different laminated electrode and their effects on the fabricated devices are discussed. Scheme 1 presents the overall concept of the dry transfer of various electrodes in the lamination processes, which will be addressed in this review.

2. Laminated perovskite solar cells (PSCs)

A majority of applied lamination methods for PSC fabrication have focused on the dry transfer of the electrodes.[77,78,80–84] In this method, the target film is first deposited onto the transfer medium and then laminated onto another stack to complete the device.[66,85,86] This target film could only be the charge transporting layers (CTLs) and/or both CTLs and back electrodes together, or CTLs and active layers.[49,87,88] Herein, we classified the laminated PSCs into two categories according to the prominent CTLs (HTLs in n–i–p structure or ETLs in p–i–n structure) to provide a more comprehensive view of the lamination methods on the electrode–CTL interface and their photovoltaic performance. However, it should be considered that the perovskite film is severely vulnerable to the lamination parameters such as the applied pressure, temperature, and the solvents/additives of electronic glue (e-glue).[66,89,90]

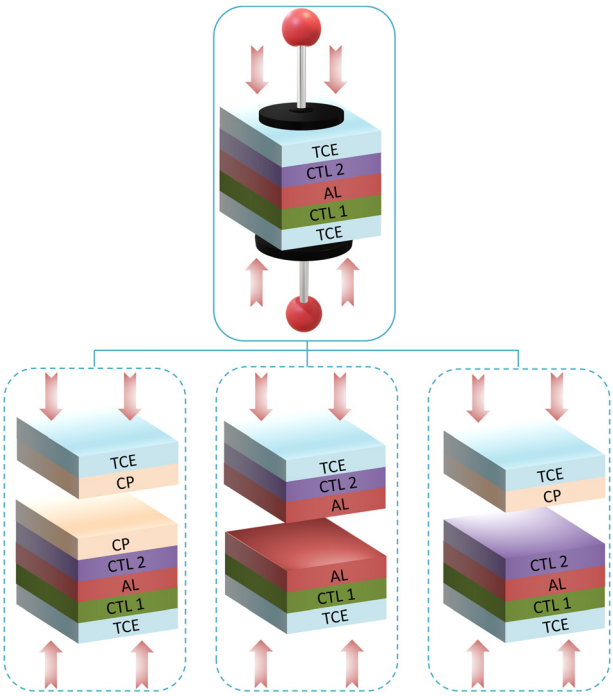

Scheme 1 Graphic illustration of the lamination of different electrodes for the fabrication of solar cells. Note: TCE is the transparent conductive electrode, CTL is the charge transporting layer, AL is the active layer, and CP is the conductive polymer.

2.1. PEDOT:PSS for PSCs

PEDOT:PSS has emerged as one of the promising hole-transporting materials (HTM) for solar cell application [135]. The high-conductivity of 1000 S cm^{-1} with appropriate work function (~5.0 eV) as well as high transparency and flexibility enable PEDOT:PSS to be used in PSCs as CTL and suitable back contact simultaneously.[91,92] However, typically, the PEDOT:PSS solution involves an aqueous or a polar solvent, which has a significantly destructive effect on the perovskite stability.[93,94] Therefore, it is crucial to develop convenient tailoring methods for the deposition or transfer of PEDOT:PSS on perovskite films.[95,96] Laminating a pre-deposited PEDOT:PSS electrode onto the perovskite films has been introduced as an efficient method to overcome this challenge. However, to enable the direct stacking of the PEDOT:PSS electrode by the lamination method, the appropriate binders are necessary to improve its mechanical strength, flexibility, and stretchability. In this regard, D-sorbitol has been broadly utilized as a cost-effective and biocompatible binder and dopant for optoelectronic applications.[53,97–99] In the initial architectures of laminated PSCs, the PEDOT:PSS layer was occasionally employed as HTL with D-sorbitol as the e-glue to stick the two stacks together.[62,77,100] In one case, the device structure of FTO glass/TiO_2/Al_2O_3/perovskite/SpiroOMeTAD/PEDOT:PSS/Ni Mesh/PET/Embedded grid was used.[100] The champion laminated cell showed a PCE of 15.5%, which was comparable to that of the fabricated device with conventional Au contact (16.7%). The achieved lower PCE might be due to imperfect

electrical contact between Spiro-OMeTAD and PEDOT:PSS layers in the laminated device.

Similarly, Troughton *et al.* fabricated flexible PSCs on the Ti foil as the primary substrate by laminating the PET film embedded in a Ni grid/conductive adhesive as a cathode onto the Spiro-OMeTAD/PEDOT:PSS layer as the HTL (Fig. 1a).[101] First, a thin layer of PEDOT:PSS was spray-coated onto the Spiro-OMeTAD as an interlayer, which acts as an HTL-to-TCA contact promoter. On the other side, the mixture of pressure-sensitive adhesive and PEDOT:PSS was blade-coated onto a PET film embedded in an Ni grid. Then, this stack was laminated onto another stack of Ti foil/TiO_2/Al_2O_3/$MAPbI_{3-x}Cl_x$/Spiro-OMeTAD/PEDOT:PSS. The thicknesses of the PEDOT:PSS interlayer is very critical for achieving the highest photovoltaic parameters. They demonstrated that using a 22 nm PEDOT:PSS interlayer leads to the best J_{sc} and FF for laminated PSC. In contrast, the higher thicknesses of this interlayer lead to faster device degradation due to the destruction of the HTL and TCA contact due to the higher water content. The PCEs of 10.3% and 12.7% were achieved for the Ti foil- and FTO glass-based devices with optimum PEDOT:PSS interlayer thickness.

In addition, Ag-NWs/TCA (PEDOT:PSS/D-sorbitol) has been used as a composited back contact electrode, which shows comparable charge transport and recombination resistances

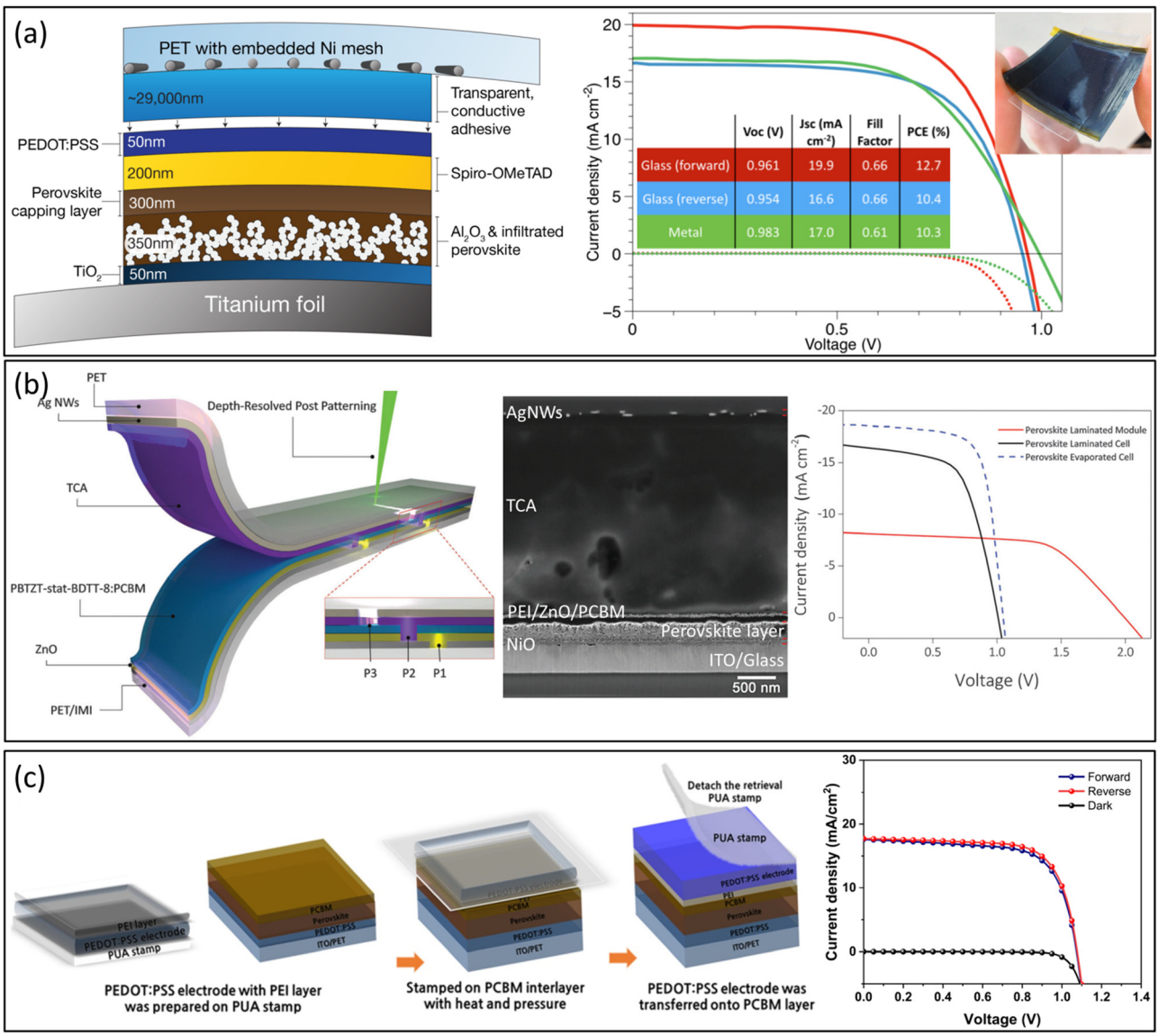

Fig. 1 (a) A schematic illustration of metal-mounted PSC and the associated target layer thicknesses, *J*–*V* characteristics of champion PSCs fabricated by metal and glass substrates, and a digital photograph of a flexible PSC on titanium foil (from left to right). Reproduced with permission.[101] Copyright 2015, Royal Society of Chemistry. (b) Device architecture of the laminated PSC module, cross-section SEM image of the laminated device on the glass substrate, and corresponding *J*–*V* curves, respectively. Reproduced with permission.[71] Copyright 2016, Royal Society of Chemistry. (c) Schematic representation of the dry stamping process of the PEDOT:PSS top electrode for semi-transparent flexible PSCs (left) and the *J*–*V* curves of the champion device on the ITO/PET substrate for both reverse and forward scans. Reproduced with permission.[106] Copyright 2020, American Chemical Society.

to the evaporated Ag electrode.[71] This electrode was used to fabricate perovskite and organic solar modules by the lamination method (Fig. 1b). Also, it was revealed that a thin layer of polyethyleneimine (PEI) on the top of ZnO nanoparticles could improve the electrical contact with the TCA in the interface of two stacks. As a result, the PCEs of 5.3% and 9.8% for organic and perovskite modules were achieved, respectively.

Furthermore, the effect of the sorbitol content in the Ag network/TCA (PEDOT:PSS/D-sorbitol) transparent electrode on the performance of laminated flexible PSCs has been evaluated.[62] With 400 mg sorbitol in 1 mL PEDOT:PSS dispersion, average performances of 6.7% and 8.8% were achieved for the abovementioned laminated electrode and FTO glass, respectively. However, a higher average PCE of 10.1% was obtained for the PSC with the Au-evaporated electrode, which might be related to the light reflection of the Au layer. Likewise, Jiang *et al.* fabricated the PSCs employing transfer-medium PEDOT:PSS PH1000 as the conducting polymer electrodes.[77] Firstly, they prepared TiO_2/$MAPbI_3$/Spiro-OMeTAD stacking on the FTO glass. Then, the back contact consisting of dried PEDOT:PSS/PDMS (polydimethylsiloxane) film was laminated upon the first stack at 90 °C, leading to a PCE of 10.9% for the final fabricated OPV device. It should be taken into account that there are several challenges in using PDMS for this purpose, including the requirements of plasma/UV-ozone treatments to enhance the film wettability before the PEDOT:PSS deposition, expensive curing agents, taking too much time for polymerization, and limitations for large-scale production. These challenges convinced researchers to substitute the PDMS transfer medium with plastic wrap.[102] In this case, Bu *et al.* prepared the PEDOT:PSS electrode on the plastic wrap for laminating atop the perovskite film.[78,84] A PCE of 10.1% was achieved for the semitransparent PSC device with optimized mesoporous TiO_2. Furthermore, using this method, the fabricated large-area semi-transparent PSC leads to a PCE of 2.9%, which could be enhanced up to 6.7% by soldering electrical wires to reduce the series resistance.

The PSS in the PEDOT:PSS structure is the poor conductive part of this polymer.[103] Therefore, PEDOT:PSS was treated with a mild HNO_3 solution to improve the performance of laminated PSCs.[104] The highly conductive e-glue (conductive adhesives) was inserted onto the stack to complete the device by a small pressure and annealing at 60 °C for 5 min, leading to enhanced V_{oc} and J_{sc} from 0.81 V and 14.3 mA cm^{-2} to 1.059 V and 22.7 mA cm^{-2}, respectively.

Dry stamping transfer has also been introduced as a suitable method for the lamination of the PEDOT:PSS (PH1000) thin film as a flexible top electrode onto the perovskite film to avoid subsequent degradation.[91,102,105] In this regard, Lee *et al.* developed a poly(urethane acrylate) (PUA) stamp to deposit the PEDOT:PSS flexible transparent electrode on the perovskite film directly.[106] First, PEDOT:PSS was coated on a PUA/Polycarbonate stamp, followed by drying. Second, a thin poly(ethyleneimine) (PEI) layer was spin-coated onto the PEDOT:PSS film to modify its work function. The prepared top electrode was laminated onto the PCBM/$FAPbI_{3-x}Br_x$/PEDOT:PSS/ITO substrate at 100 °C using a roller, and then the PUA/Polycarbonate film was detached (Fig. 1c). Therein, reproducible semi-transparent highly-flexible PSCs with over 13% PCE were obtained.

Laminating two different half-stacks perovskite films is another approach for the fabrication of PSCs: Dunfield *et al.* fabricated two half-stacks of the TCO/SnO_x/perovskite and TCO/NiO_x/perovskite by the solution-processed method separately.[54] As shown in Fig. 2a, the PSC was completed by laminating them together at 150 °C under 300 psi (=2.06 MPa) pressure, leading to a PCE of 10.6%. Nevertheless, the low average PCE of 9.6% for these devices was mainly attributed to the higher series resistance (R_S = 59 Ω), which caused resistive losses through the wide TCO on each side.

Inspired by the DSSCs sandwich device structure, the two TCO electrodes can be used as front and back electrodes to fabricate the PSC with self-encapsulation features to protect the devices from moisture and improve the device stability.[56,107–109] Using this architecture, Heo *et al.* fabricated semi-transparent planar sandwich PSCs with almost a hysteresis-free PCE of 15.8% and over 20 days of stability (5% dropped PCE) without any extra encapsulation.[56] They used semi-transparent FTO glass/TiO_2/$MAPbI_3$/HTL and ITO/PEDOT:PSS as the first and second stack, respectively. These two stacks were pressurized by a double clip and then dried to complete the device structure. To improve the physical contact between the two stacks, a drop of HTL (P3HT or PTAA) was cast onto the perovskite films before the lamination process (Fig. 2b). The average PCEs of 12.8% and 15.8% was achieved for fabricated PSCs with P3HT and PTAA as the HTLs, respectively.

Dunlap-Shohl *et al.* explored the behavior of the perovskite film and other layers under severe lamination conditions, *i.e.*, high pressure and temperature.[90] Therein, they applied a rapid lamination method to complete the device in 5 minutes. Based on the XRD studies, they demonstrated that applying pressure during the $MAPbI_3$ annealing could help the layers to endure high temperatures in the lamination process. The Spiro-OMeTAD/D-sorbitol/PEDOT:PSS/ITO stack was glued to the ITO/SnO_2/PCBM/$MAPbI_3$/Spiro-OMeTAD stack at 120 °C and 500 psi (=3.44 MPa) pressure to produce a bifacial PSC, achieving a PCE up to 12% (Fig. 2c). Recently, the same research group further boosted the performance and stability of the laminated bifacial PSCs using albedo light in the bifacial structure of PSCs and optimizing the HTL thickness.[110] Similarly, the first stack of glass/ITO/SnO_2/$MAPbI_3$/undoped Spiro-OMeTAD and the second stack of glass/ITO/PEDOT:PSS/D-sorbitol were pressed at 100 °C and 2000 psi (=13.8 MPa). The optimization of functional additive (FN-Br (3,3′-(2,7-dibromo-9*H*-fluorene-9,9-diyl)bis-(*N*,*N*-dimethylpropane-1-amine))) concentration in the HTL solution adjusted the Fermi level of Spiro-OMeTAD, leading to improved V_{oc} and FF from 0.98 to 1.08 V and from 0.65 to 0.75, respectively. As a result, a PCE of 15% with 0.93 bifaciality was achieved for rapid laminated PSC in one minute, as well as acceptable stability by maintaining 75% of the original PCE under continuous illumination at 50% RH for 100 h.

In the case of PEDOT:PSS lamination, laminating the PEDOT:PSS film in the p–i–n device is not very common. Since its aqueous

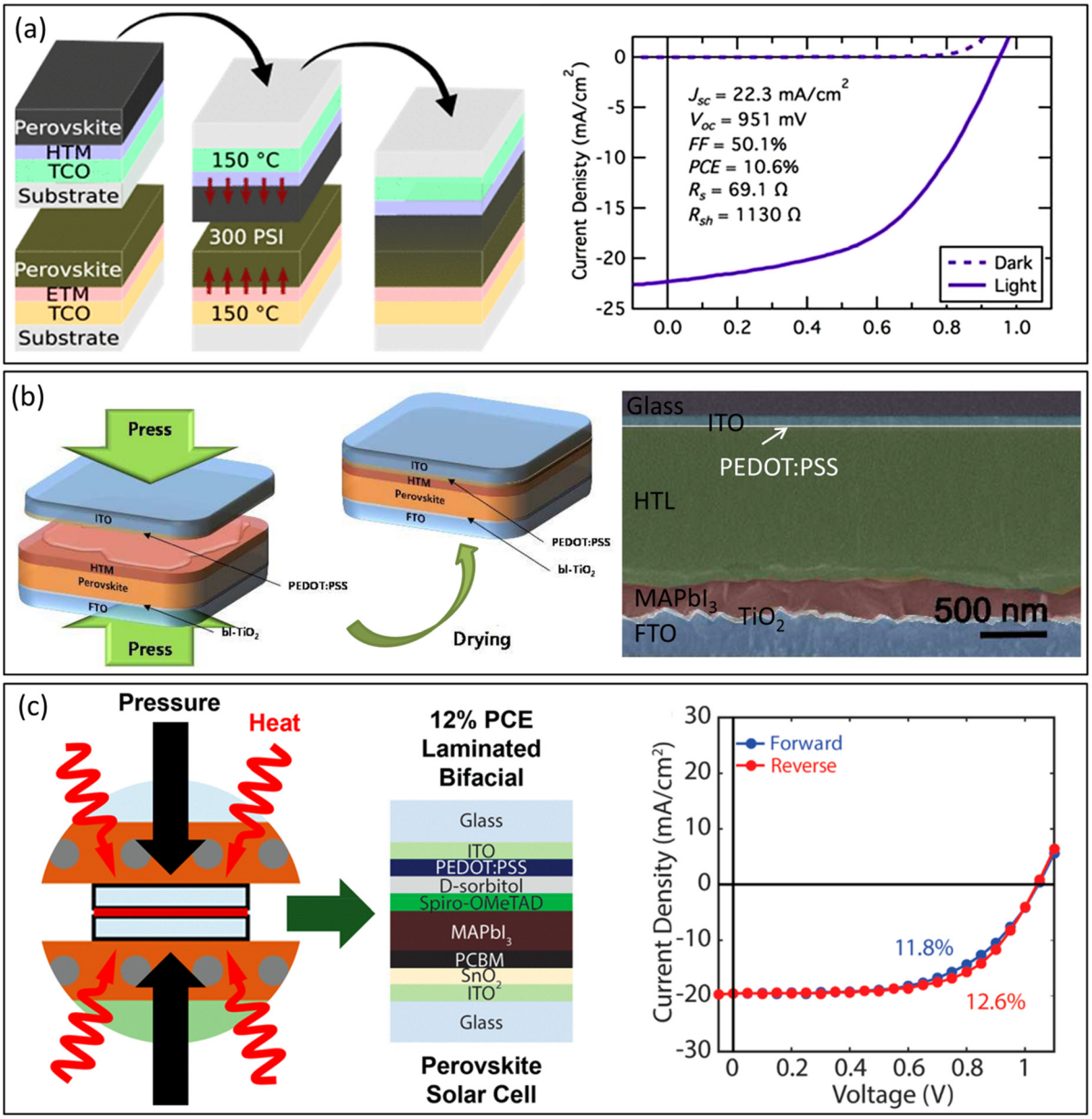

Fig. 2 (a) Schematic presentation showing the fabrication of half stacks, lamination procedure, and the structure of laminated PSC device (left) and the *J*–*V* curve of champion PSC with corresponding parameters (right). Reproduced with permission.[54] Copyright 2018, American Chemical Society. (b) Schematic illustration for device fabrication and architecture of $MAPbI_3$ planar sandwich solar cell (left) and cross-sectional SEM images of full sandwich PSC (right). Reproduced with permission.[56] Copyright 2015, Royal Society of Chemistry. (c) Schematic description of the lamination method and the resultant laminated PSC device (left) and the *J*–*V* curves of the champion device, collected using a 1 s measurement delay and illumination through the ETL (right). Reproduced with permission,[90] Copyright 2019, American Chemical Society.

dispersion could be deposited by conventional coating methods and annealed as HTLs before the perovskite layer, it is not destructive to the overall performance of the PSC devices.

In an overall view, the utilization of PEDOT:PSS in laminated semitransparent PSCs has been described. These methods could be used to fabricate large-area, high-efficiency, and low-cost semitransparent PSCs with high stability. They mainly involve manufacturing an e-glue or TCA to stick the two prepared half-stacks (one of them includes PEDOT:PSS) and highly conductive composites with metal grids to be directly transferred onto the HTL *via* transfer media. The applied pressure plays a key role in the lamination process. The higher pressure ensures a perfect contact interface between the perovskite and the dry-transferred top layers and reduces detachment, improving the charge transfer and performance of the devices. However, monitoring the inserted pressure is necessary to find the optimized value. As yet, the highest PCE was reported to be 15.77% for laminated planar PSCs with a bifacial (sandwiched) configuration using PEDOT:PSS as a highly conductive adhesive layer to stick the top ITO.[110]

2.2. Carbon materials for PSCs

So far, various carbonaceous materials with different morphologies such as carbon black, graphite, carbon nanotubes (CNTs), and graphene have been used for PSCs due to many advantages such as low cost, hydrophobicity, high conductivity, flexibility, chemically inert nature, and appropriate work functions.[111,112] Moreover, unlike conventional metal back contacts, carbon materials possess a relatively high specific surface area with suitable energy level, making them applicable as HTL and/or back contact films in PSCs.[113–116] The interface compatibility between the carbon and the perovskite films is crucial, especially for the HTL-free carbon-based PSCs. For instance, the layered and foliated nature of graphite tends to create a spatial distance from the perovskite film. This challenge could be tackled through solvent or additive engineering to achieve an ideal carbon/perovskite interface.[117,118] However, inducing the HTL in carbon-based PSC architectures reduces hole recombination at this interface. Besides, the sheet resistance of the carbon electrodes also affects the performance of the PSCs by reducing the V_{oc} and FF parameters.[53,119]

The carbon pastes could be prepared by adding a suitable binder to carbon nanomaterials, followed by a sonication or homogenizer process. This carbon paste could be deposited on a substrate to produce a nanocarbon-binder film. After that, this carbon film undergoes either of the two changes to produce free-standing or self-standing carbon films. In the first approach, the solvent-exchange process, the carbon film is immersed in an appropriate solvent, *i.e.*, ethanol, to exchange the solvent medium, followed by drying in ambient air and finally peeled off from the substrate.[120,121] In the second approach, the carbon film is annealed/dried, usually on a hot plate, to evaporate the solvent and then peeled off the substrate.

The solvent-exchange process in carbon paste has been introduced by Zhang *et al.* to avoid damaging the perovskite film during the fabrication of PSCs, producing two kinds of blade-coated carbon electrode films with different qualities (see Fig. 3a).[122] The press transfer during the lamination process caused decreasing sheet resistance of the carbon film from 424 to 58 Ω sq^{-1}. As a result, the laminated carbon-based PSC devices showed 19.2% PCE, whereas blade-coated carbon-based PSCs demonstrated a PCE of 15.2%.

The hot-pressing of the free-standing carbon films for the fabrication of the carbon-based PSCs was reported by Yang *et al.*[123] They used this method for a triple cation-based PSC planar structure with CuSCN/Spiro-OMeTAD as the HTLs. They benefited from the solvent-removing of carbon paste through the immersion of the film in ethanol,[122] followed by N_2-drying, peeling off the carbon film from the substrate, and pressing the carbon electrode directly onto the HTL. The sheet resistance and morphology of the prepared carbon films and the photovoltaic performance of the PSCs were studied by applying different temperature ranges of 22 °C, 40 °C, 60 °C, and 80 °C at a constant pressure insertion of 30 MPa for 3 min. It was demonstrated that the temperature increase leads to lower average R_s (13.78 $\pm$ 1.03 Ω) and lower hysteresis index (0.007 $\pm$ 0.010), as well as a higher average V_{oc} (1.08 $\pm$ 0.01 V), J_{sc} (20.2 $\pm$ 0.5 mA cm^{-1}), FF (66.5 $\pm$ 1.0%), and thus PCE (14.5 $\pm$ 0.4%) of the fabricated PSCs. The champion PCE of 15.3% retained 93% of its initial amount after 80 days under 70% RH.

The effect of ethanol solvent interlacing time from the carbon paste in the solvent-exchange process on the carbon film properties and thus ultimate C-based PSC performance has recently been studied by Passatorntaschakorn *et al.*[124] They demonstrated that the excess binder containing C═O functional group in the carbon films could be effectively removed after 2 h of immersing carbon films in the ethanol, resulting in a more uniform and conductive electrode. The improved charge transfers between carbon and Spiro-OMeTAD layer lead to a PCE of 12.2% for the laminated PSC.

The performance of free-standing hybrid graphene/dry-spun CNT films as multifunctional electrodes for laminated PSCs has also been examined.[118] First, the double-layer graphene/Cu stacked layer was prepared, and then the CNT was coated *via* the dry-spinning method.[125] After that, Cu was etched to obtain a hybrid graphene/graphene/CNT free-standing film. This film was scooped by a PTFE transfer medium and transferred onto the FTO/TiO_2/perovskite/Spiro-OMeTAD stack utilizing a roller. The hybrid graphene (4-layers)/CNT (8-layers) film demonstrated the best conductivity and performance, leading to a PCE of 15.3% with 86% retention of the initial value after 500 h at 50% RH without encapsulation.

Very recently, a conductive cloth composed of polyester woven fabric with Ni/Cu coatings on yarn was employed as a support substrate by Peng *et al.*[126] They used a similar solvent-exchange process for carbon film. As shown in Fig. 3b, after the blade-coating of carbon paste on the conductive cloth, the peeled-off wet composite film was soaked in ethanol for the solvent-exchange process. The mesh structure of the carbon/conductive cloth composite promotes the diffusion of the ethanol molecules into this layer and facilitates ethanol evaporation afterward. The resulting composite carbon electrode was applied to fabricate both rigid and flexible PSCs. Also, this film was compared to other obtained carbon films such as bare self-adhesive carbon film, carbon/graphite paper film, and carbon/aluminum foil. As a result, the fabricated PSCs with carbon/conductive cloth film demonstrated low resistance with high flexibility, achieving remarkable PCEs of 19.36%, 15.37%, and 14.05% for rigid, small-area flexible (0.1 cm^2), and large-area flexible (1 cm^2) substrates, respectively.

As another method, FTO glass was placed at a constant distance of 2 cm above a burning candle to collect the soot at different times of 10, 15, and 20 s.[127] The material characterization analyses confirmed the graphite carbon nature of the formed film. The resulting spongy carbon film on the FTO substrate was pressed on the Spiro-OMeTAD layer as the back contact to complete the PSC device, leading to a maximum PCE of 4.24%.

Coal-based carbon (Coal-C) electrode has also been introduced for low-cost laminated HTL-free PSCs.[128] In this approach, Coal-C powder, acetylene black, and PVAc were

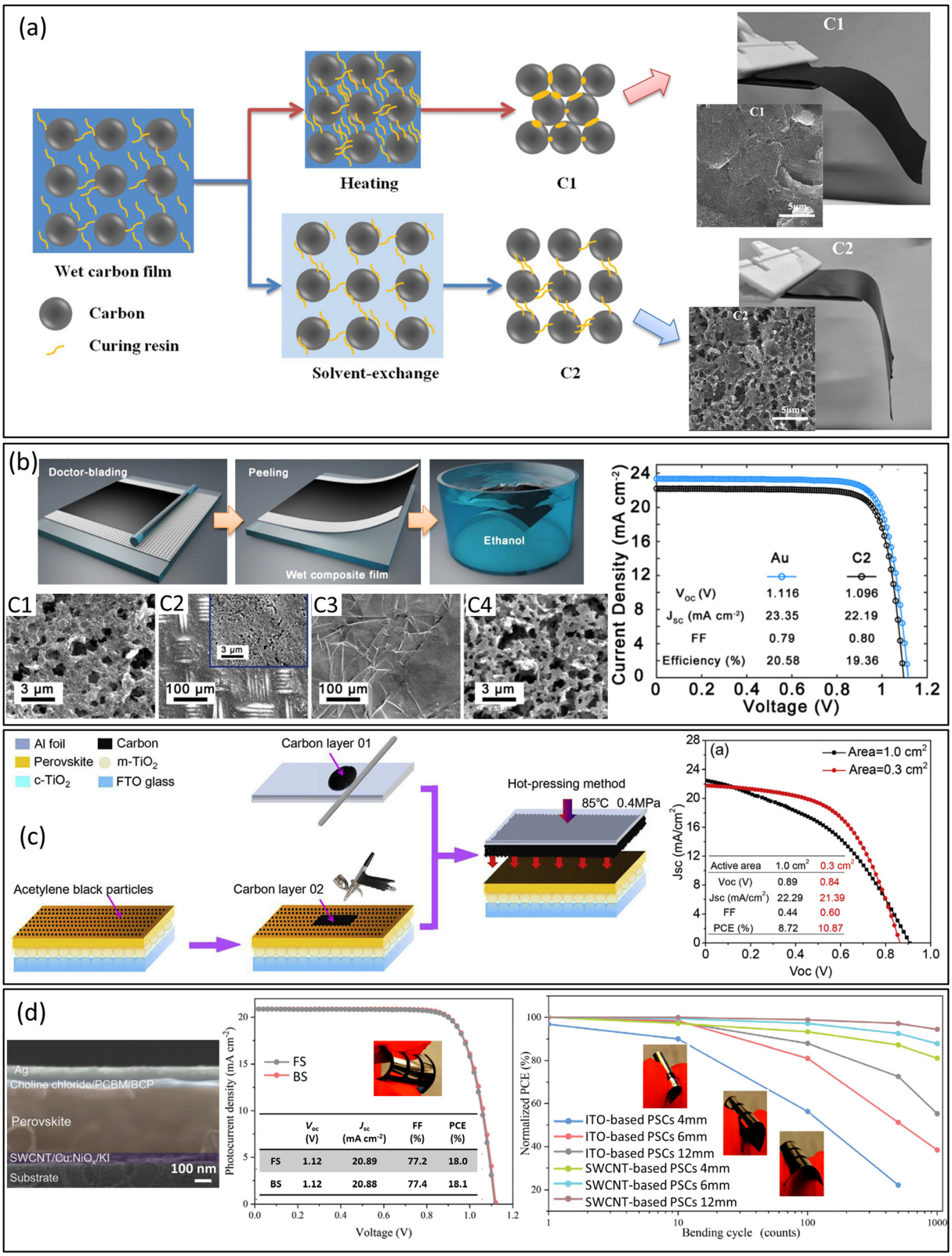

Fig. 3 (a) Microscopic curing mechanism during C1 and C2 film formation. Digital photographs of the mechanical flexibility of C1 and C2 films with the surface SEM images of C1 and C2 films. Reproduced with permission.[122] Copyright 2013, Wiley-VCH. b) Schematic drawing of the carbon film preparation using the blade-coating method and solvent-exchange process. From left to right: the SEM morphology of the backside of the bare self-adhesive carbon film (C1), carbon/conductive cloth film (C2), carbon/graphite paper film (C3), and carbon/aluminum foil film (C4) after removing the aluminum substrate. *J*–*V* curves of champion PSCs based on gold and C2 carbon film. Reproduced with permission.[126] Copyright 2021, Elsevier. (c) Schematic presentation of Coal-C electrodes fabrication process and *J*–*V* curve of PSCs fabricated of Coal-C electrodes. Reproduced with permission.[128] Copyright 2013, Elsevier. (d) Cross-sectional SEM images of PSC fabricated by SWCNT. *J*–*V* characteristics of SWCNT-based flexible PSC and bending test of ITO- and SWCNT-based flexible PSCs with a different bending radius of 4, 6, and 12 mm. Reproduced with permission.[134] Copyright 2021, Wiley-VCH.

mixed in chlorobenzene, and then the mixture was blade-coated on an Al foil substrate (Fig. 3c). On the other side, the second carbon paste was sprayed on the perovskite film, followed by an annealing process to achieve the FTO/c-TiO_2/m-TiO_2/perovskite/carbon second stack. The first carbon film was hot-pressed on the second stack at 85 °C under 0.4 MPa pressure for 50 s. The fabricated PSC with 20 mg mL^{-1} acetylene black paste showed the lowest series resistance (R_s) of 3.73 Ω, achieving a PCE of 10.87%.

Wei *et al.* prepared different ratios of graphite flake and carbon black powder in polyvinyl acetate to optimize the carbon paste.[129] After making the carbon paste with an optimal weight ratio of 3 : 1 for graphite:carbon black powder by a low-temperature and straightforward process, the carbon film was fabricated using a blade-coating method on a Teflon film/Al foil, followed by drying and peeling off. Thereafter, this carbon film was directly hot-pressed at various pressures of 0.15, 0.25, and 0.40 MPa onto the perovskite film, reaching a PCE of 13.53% for the optimal pressure of 0.25 MPa. Moreover, this carbon-based PSC showed only a 5% PCE drop (from 13.53% to 12.87%) after 20 days under ambient conditions, while the Au-based PSC showed a 21% PCE drop (from 10.69% to 8.55%) under the same conditions.

As the first study on graphene, You *et al.* laminated multi-layer graphene as the top electrode onto the perovskite/HTL film to fabricate PSCs.[130] The multi-layer graphene was synthesized on a copper foil by the CVD method and was then transferred onto the poly(methyl methacrylate) (PMMA)/PDMS film as the transfer medium. Then, this PDMS/PMMA/graphene stack was peeled-off and laminated onto the FTO/TiO_2/$CH_3NH_3PbI_{3-x}Cl_x$/Spiro-OMeTAD/PEDOT:PSS stack to complete the PSC. Besides, for improving the conductivity and transmittance of the graphene film, a thin film of PEDOT:PSS was spin-coated on the graphene surface, which reduced the sheet resistance of two-layer graphene to 140 ± 35 Ω sq^{-1} and reached up to 90% transmittance. Consequently, the maximum PCEs of 12.02% and 11.65% were achieved for semitransparent PSCs with FTO and graphene illumination sides, respectively.[130]

As mentioned in the previous section, CNTs are desirable for photovoltaics electrodes since they can provide the R2R deposition process due to their flexibility and semitransparency properties.[131,132] Firstly, Aitola *et al.* used single-wall carbon nanotube (SWCNT) films for PSCs fabrication using the press-transfer lamination method.[133] First, a filter coated with SWCNT film was pressed onto the perovskite film. Then, the filter was peeled-off, and chlorobenzene was dropped onto the film to densify it. Another layer of SWCNT was laminated on top of the previous layer to decrease the sheet resistance, leading to reduced resistance from 43 to 13 Ω sq^{-1}. The hole transport contact was finalized by drop-casting the Spiro-OMeTAD solution onto the resultant SWCNT film. As a result, the laminated PSC with SWCNT back contact showed a PCE of 16%, comparable to Au back contact-based PSC with a PCE of 18%. Interestingly, the SWCNT-based PSCs showed high-temperature stability at 60 °C under an N_2 atmosphere over 580 h with slight efficiency loss, while the Au-based PSCs showed only 140 h stability under the same conditions. Recently, Zhang *et al.* explored the effects of HNO_3 treatment on the $CuNiO_x$-doped SWCNTs layer. They used a simple dry-transfer method to laminate the resulting SWCNT films on both rigid and flexible substrates and fabricate inverted PSCs.[134] The fabricated PSCs with HNO_3-treated Cu:NiO_x-doped SWCNT showed champion PCEs of 19.0% and 18.0% on rigid and flexible substrates, respectively. Moreover, the SWCNT-based flexible PSC could retain 85% of its initial PCEs after bending 1000 times at a 6 mm radius (Fig. 3d).

In summary, free-standing carbon films from carbon pastes, CNTs, and graphene sheets applied in dry-transfer lamination could meet the PSCs R2R production requirements, including low costs, good interfacial contacts, high efficiency, and stability. In terms of the performance, the highest reported PCE of PSCs based on laminated carbon films onto the HTL as the top contact reached 19.2% in 2019[122] and 19.36% in 2021.[126] For the laminated SWCNT films as the bottom contact in the inverted PSC structure, 19.0% PCE was achieved.[134]

2.3. Metal back contacts for PSCs

The low electrical resistance of metal nanostructures such as silver nanoparticles (Ag NPs) and silver nanowires (Ag NWs) make them suitable as back contact materials for PSCs.[135–137] However, the Ag NPs inks require sintering at high temperatures to provide better conductivity, which most of the time leads to silver diffusing into the layers beneath and subsequently damaging the perovskite structure.[138–140] To address this challenge, Trinh *et al.* spin-coated the Ag NPs ink onto a PET substrate and annealing, followed by spin-coating the PEDOT:PSS/D-sorbitol solution on top as the first stack. Then, they laminated the first stack onto the second stack consisting of FTO/c-TiO_2/m-TiO_2/$CH_3NH_3PbI_3$/Spiro-MeOTAD layers at 120 °C for 10 min, followed by finger pressure pressing to complete the device.[141] The laminated PSCs therein attained an average PCE of 10.03%, which was close to the thermally-evaporated Ag electrode-based device with 11.9% PCE. Very recently, the Ag NWs top electrode was laminated using PEI as a sticky glue with several advantages such as good adhesion, surface modification of the electrode, and protective coating, which suppressed the chemical reaction between silver and the perovskite film (Fig. 4a).[142] First, the Ag NWs network was sprayed on the glass substrate coated by the self-assembly octadecyl trichlorosilane (OTS) monolayer with low surface energy (donor). Then, the prepared electrode, *i.e.*, glass/OTS/Ag NWs/PEI, was laminated onto the ITO/PEDOT/perovskite/PCBM stack by cold isostatic pressing at 8 MPa for 10 min, leading to a PCE of 12%.

In a versatile lamination method, Schmager *et al.* reported the hot-pressing lamination of two half-stacks consisting of ITO/SnO_2/perovskite/PTAA and PEN foil/evaporated Au/sputtered NiO_x HTL, respectively.[63] The lamination was performed in the pressure and temperature ranges from 0 to 200 kN and 60 to 105 °C, respectively. The critical point in their lamination strategy was a thin PTAA buffer layer at the perovskite/NiO_x interface, which improved the mechanical and electrical

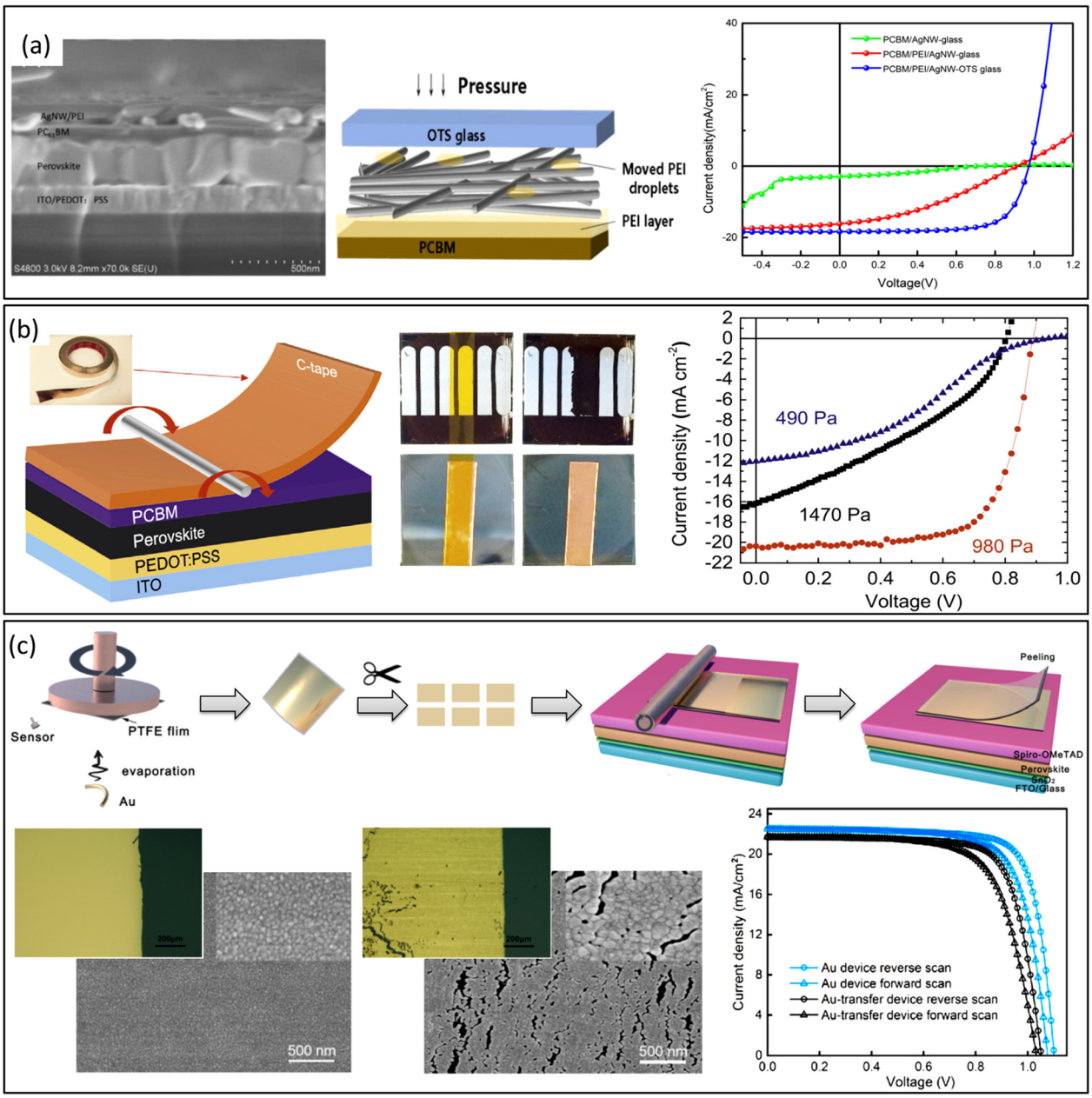

Fig. 4 (a) Cross-sectional SEM images of AgNW-laminated PSC. Schematic description of the PEI movement during pressure duration. *J*–*V* curves of the PSCs with different laminated top electrodes. Reproduced with permission.[142] Copyright 2021, Elsevier. (b) Schematic illustration of the device structure of the R2R lamination process. Inset is the photograph of the Cu conductive tape. Digital photographs of a PSC with and after peeling off the Kapton tape on an evaporated Al electrode (top row) and a laminated PSC with and after peeling off the Kapton tape (bottom row). *J*–*V* curves of the laminated PSCs made by different pressures. Reproduced with permission.[143] Copyright 2015, Elsevier. (c) Schematic representation of the transferring pressed Au electrode on PSC devices. Optical microscopy images with the top-view SEM images of evaporated Au (left) and Au-transfer-based PSC devices (right). *J*–*V* curves of the best PSCs based on Au and Au-transfer electrodes. Reproduced with permission.[85] Copyright 2021, Elsevier.

contact by filling the remaining holes at the interface. Hence, PTAA-based PSC showed a higher FF of 70%, a lower R_s of 60 Ω, and a higher PCE of 14.6% compared to the devices without the PTAA buffer layer with an FF of 60%, an R_s of 180 Ω, and a PCE of 13.2%. The self-encapsulated architecture of the presented lamination method also blocked oxygen and moisture, leading to enhanced stability. The structures based on rigid semi-transparent, opaque flexible, and semi-transparent flexible PSCs showed PCEs of 11.5%, 11.3%, and 8.8%, respectively. This method could be adaptable for tandem or module applications.

The application of economic and commercial conductive tapes (C-tapes) consisting of Cu foil support and conductive acrylic adhesive with embedded micrometer-size Ni particles as the top electrode in the inverted PSCs was reported by Shao *et al.*[143] (Fig. 4b). They demonstrated that applying 980 Pa

pressure on the C-tape during the lamination process is necessary to achieve desirable contact with the underlayer, achieving a champion PCE of 12.7%. In terms of stability, the PCE of the laminated device dropped from 12.3% to only 11.0% after ten days under ambient conditions, while the non-laminated counterpart dropped severely from 14.6% to 3.4%, demonstrating the capability of C-tapes for impeding moisture and humidity from entering the device.

Low-cost transparent electrode based on PET/Cu Grid: PH1000 was fabricated by forming the Cu honeycombs structure on a photoresist film and lifting it off to leave the Cu as bottom contact in inverted flexible PSCs.[144] They could acquire 13.58% PCE and 90% stability with more than 1000 bending cycles of 5 mm curvature.

Recently, Li *et al.* developed a solvent and vacuum-free press-transferring of Au back-contact to fabricate PSCs.[85] In this case, 80 nm Au was evaporated on the PTFE films to achieve the Au/PTFE film. Then, as schematically shown in Fig. 4c, the Au/PTFE stack pressed by a glass rod onto another stack consisted of FTO glass/SnO_2/perovskite/Spiro-OMeTAD, followed by the peeling off the PTFE film to complete the PSC. Therein, PCEs of 17.4% and 19.2% were achieved for the Au-laminated Au thermally-evaporated PSCs, respectively. They mentioned that the lower PCE for the laminated device might be due to higher sheet resistance, insufficient coverage of the Au film, and random microcracks in Au-transfer.

Overall, the laminated metal back contacts in PSCs mainly involved the press-transferring of Ag NWs, commercial Cu adhesives, and Au films with convenient transfer media. Moreover, these high-conductive materials could be combined with other materials to produce composite electrodes for lamination usages, as shown in previous sections. The highest PCEs of 17.4% and 12.5% were obtained for n–i–p and p–i–n metal contact-laminated PSCs, respectively.[85,143]

Table 1 presents device configuration, materials, and photovoltaic characteristics for different laminated PSCs that have been discussed so far based on the literature review.

3. Laminated organic photovoltaics (OPVs)

Similar to PSCs, traditional solutions or vacuum evaporation-assisted methods are still very popular for depositing different layers in OPVs.[99,146] However, besides the high fabrication costs of these methods, diffusing different materials into the underneath organic layers and damaging the organic layers lead to low PCEs and stabilities. Therefore, it is quite necessary to introduce better device fabrication methods that are more compatible with scalable R2R processes.[90,91,139–143] The lamination of pre-deposited layers on different stacks has been introduced as a promising method to fabricate highly efficient and stable OPVs. Similar to the PSCs section, here, we classified the laminated OPVs based on laminating charge-transporting layers (CTLs) and/or both CTLs and back contact electrodes.

3.1. PEDOT:PSS for OPVs

The PEDOT:PSS has been introduced as the most widespread polymeric alternative back contact for ITO-free and/or metal-free OPVs.[102,147] Firstly, Huang *et al.*[72] studied the lamination of flexible electrodes to fabricate semitransparent OPVs. They laminated the PEDOT:PSS (PH1000):D-sorbitol (E-glue) film onto the active organic layer at the optimized temperature of 110 °C for 10–15 minutes, leading to a PCE of 3%. Similarly, Yuan *et al.*[148] coated the PEDOT:PSS:D-sorbitol as an e-glue on the PEN/Ag substrate, followed by lamination onto the ITO/$CsCo_3$/P3HT:PCBM stack at 100 °C and 10–50 KPa. The laminated device showed a PCE of 4.0%, comparable to the achieved PCE of 3.6% for regular inverted OPV with MoO_3/Ag anode.

Besides, the nanoparticle (NP) interlayer for the lamination of OPVs has been introduced to achieve desired electrical and mechanical contact.[72,75,149] For example, Lu *et al.* implemented insulating barium titanate ($BaTiO_3$) NPs into the active layer solution as a spacer to improve the mechanical stability of the inverted OPVs.[150] In this case, the laminated flexible OPVs with $BaTiO_3$ NPs presented a PCE of 3.79% with high endurance and stability under high pressure and large bending curvature. Although a similar PCE of 3.81% was achieved for the device without the NPs, however, with a severe current leakage under pressure and bending of more than 40°.

The dry stamp transfer lamination has been introduced as a more promising method compared to glue-based lamination for the fabrication of OPVs, which solve the wettability challenge of the PEDOT:PSS film during the device fabrication.[80,151–153] In this approach, the e-glue (mainly consisting of PEDOT:PSS with D-sorbitol) was spin-coated on an elastomeric stamp directly, followed by lamination under pressure onto another half stack at a specific temperature, resulting in the transfer of the PDEOT:PSS layer onto the device.[151–153] As an example of this method, Gupta *et al.* deposited PEDOT:PSS directly onto plasma-treated PDMS as the stamp, followed by lamination onto the rest of the device stack and annealed at 80–90 °C for 2 min. After cooling down the substrate, the PDMS was mechanically peeled-off. Nevertheless, to enhance the conductivity and reduce the sheet resistance of PH1000, 100 nm thick Ag lines were evaporated on it as the busbars through the shadow mask (Fig. 5a, type A and B). As a result, the laminated OPVs in n–i–p and p–i–n configurations showed PCEs of 3.25% and 2.12%, respectively.

Although the fabrication of flexible OPVs by the lamination method is challenging due to flexible substrate electrodes for both top and bottom contacts, they presented significant performances compared to rigid TCO contacts counterparts.[75,102,154] For example, Zhou *et al.* fabricated recyclable flexible OPVs based on cellulose nanocrystal (CNC) substrates with the CNC/Ag/PEI/P3HT:ICBA/PH1000 device configuration.[153] Similarly, the PEDOT:PSS PH1000 was deposited on the PDMS transfer medium. On the other side, the surface of the photoactive layer (P3HT:ICBA) was exposed to flash-instant O_2/plasma to become more hydrophilic, resulting in easier PEDOT:PSS transfer without further thermal annealing or air drying. The resulting laminated-PSC achieved

Table 1 The summarized device configuration, materials, and photovoltaic characteristics of the laminated PSCs. PCEi = initial PCE

Configuration	Laminated electrode	V_{oc} (V)	J_{sc} (mA cm^{-2})	FF	PCE_i (%)	Area (cm^2)	Stability	Ref.
FTO/c-TiO_2/m-TiO_2/$MAPbI_3$/CNTs	CNTs	0.88	15.5	0.51	6.8	0.16	N/A	58
FTO/c-TiO_2/m-Al_2O_3/$MAPbI_{3-x}Cl_x$/Spiro-OMeTAD/PEDOT:PSS/PEDOT:PSS:acrylic adhesive/Ni grid/PET	PEDOT:PSS:acrylic adhesive/Ni grid/PET	0.95	20.7	0.64	13.3	0.06	N/A	100
Titanium foil/c-TiO_2/m-Al_2O_3/$MAPbI_{3-x}Cl_x$/Spiro-OMeTAD/PEDOT:PSS/PEDOT:PSS:acrylic adhesive/Ni grid/PET	PEDOT:PSS:acrylic adhesive/Ni grid/PET	0.99	17.0	0.61	10.3	0.24	93% of PCE_i after 200 bend cycles	101
FTO/c-TiO_2/m-TiO_2/$MAPbI_3$/Spiro-OMeTAD/PEDOT:PSS:D-sorbitol/PDMS/PMMA/graphene	Graphene	0.96	19.2	0.67	12.3	0.24	~88% of PCE_i under a bias voltage of 0.72	130
FTO/c-TiO_2/m-TiO_2/$MAPbI_3$/Spiro-OMeTAD/PEDOT:PSS	PEDOT:PSS/Plastic wrap	0.97	16.0	0.65	10.1	0.06	N/A	84
FTO/c-TiO_2/m-TiO_2/$MAPbI_3$/Spiro-OMeTAD/PEDOT:PSS (PH 1000)	PEDOT:PSS (PH 1000)	0.97	16.4	0.57	6.05	0.044	N/A	77
FTO/c-TiO_2/$MAPbI_3$/HTL/PEDOT:PSS/ITO	PEDOT:PSS/ITO	0.94	18.0	0.75	12.80 (P3HT)	N/A	~95% of PCE_i after 20 days in the air at 50 °C	56
		1.10	19.3	0.75	15.80 (PTAA)			
ITO/PEDOT:PSS/$MAPbI_3$/PCBM/Cu Kapton tape	Cu Kapton tape	0.88	12.1	N/A	12.7	0.10	94% and 98.7% of PCE_i in N_2 and air (15% RH), respectively, after 10 days	143
FTO/c-TiO_2/$MAPbI_3$/Carbon	Carbon film	1.0	21.3	0.63	13.5	0.08	95% of PCE_i after 20 days in the air	129
FTO/c-TiO_2/$MAPbI_{3-x}Cl_x$/Spiro-OMeTAD/PEDOT:PSS:Sorbitol/Ag network	$MAPbI_{3-x}Cl_x$	1.05	20.7	0.61	13.2	0.1	N/A	86
ITO/NiO/$MAPbI_3$/PCBM/PEI/PEDOT:PSS:Sorbitol/Ag NWs/PET	PEDOT:PSS–Ag nanowire composite	1.01	16.4	0.59	9.8	0.15	95% of PCE_i after over 100 h in N_2	71
FTO/c-TiO_2/m-TiO_2/m-SiO_2/$MAPbI_3$/MWNTs	MWNTs	0.93	21.3	0.59	11.6	0.1	N/A	87
FTO/c-TiO_2/m-TiO_2/$MAPbI_3$/Spiro-OMeTAD/Carbon	The soot of a burning candle (carbon)	0.82	12.3	0.42	4.2	0.1	N/A	127
Glass or PDMS substrate/TFSA-doped Graphene/PEDOT:PSS/$FAPbI_{3-x}Br_x$/PCBM/Al	PDMS or glass substrate/TFSA-doped Graphene	1.07	22.7	0.78	18.9 (Glass)	N/A	95% of PCE_i after 1000 h in 30% RH at 60 °C	145
		1.07	22.1	0.77	18.2 (PDMS)			
FTO/c-TiO_2/m-TiO_2/FAMAPbIBr/Spiro-OMeTAD/Carbon	Carbon	1.08	23.3	0.76	19.2	0.1	95% of PCE_i after 1000 h in ambient condition	122
Ti substrate/$MAPbI_3$/PTAA/graphene/PDMS counter electrode	graphene/PDMS counter electrode	1.08	18.7	0.74	15.0	2.5	N/A	88
PET/TFSA-Graphene/PEDOT:PSS/PTAA/$MAPbI_3$/ZnO/TETA-Graphene/PET	PET/TFSA-Graphene/PEDOT:PSS	0.95	18.0	0.65	11.16 (with mirror)	1.0	0.79% of PCE_i at R = 12 mm bending	65
		0.97	16.8	0.66	10.7 (w/o mirror)		97.6% of PCE_i at R = 12 mm bending	
FTO/c-TiO_2/m-TiO_2/CsFAMAPbIBr/Spiro-OMeTAD/spray carbon/doctor blading coal-carbon	doctor blading coal-carbon	0.84	21.4	0.60	10.8	0.3	85% of PCE_i after 120 h in 30% RH in the air	128
FTO/SnO_2/$Cs_{0.05}(MA_{0.17}FA_{0.83})_{0.95}Pb(I_{0.83}Br_{0.17})_3$/Spiro-OMeTAD/PEDOT:PSS:Zonyl:D-sorbitol/*n*-PEDOT:PSS/PDMS	PDMS/*n*-PEDOT:PSS/PEDOT:PSS:Zonyl:D-sorbitol	1.06	22.7	0.68	16.4	N/A	93% of PCE_i after 7 days in 25% RHa in the dry box	104
FTO/c-TiO_2/m-TiO_2/$Cs_5(MA_{0.17}FA_{0.83})_{95}Pb(I_{0.83}Br_{0.17})_3$/Spiro-OMeTAD/SWCNT+ Spiro-OMeTAD	SWCNT film	1.12	21.0	0.71	16.6	0.16	95% of PCE_i after 140 h at 60 °C in N_2	133
FTO/c-TiO_2/m-TiO_2/$MAPbI_3$/Spiro-OMeTAD/hybrid graphene/CNT films	4-Layer graphene-/8-layer CNT film/PTFE foil	1.07	21.8	0.66	15.3	0.09	86% of PCE_i after 500 h in 50% RH	118
ITO/C_{60}/$MAPbI_3$/SWCNT + Spiro-MeOTAD	CNT film + spiro-MeOTAD	1.08	23.8	0.66	17	N/A	80% of PCE_i after 2200 h in the air	57
FTO/SnO_2/PCBM/$MAPbI_3$/Spiro-OMeTAD/D-sorbitol/PEDOT:PSS/ITO glass	Sorbitol/PEDOT:PSS/ITO glass	1.01	20.5	0.54	12.6	N/A	N/A	90
ITO/SnO_2/$Cs_{0.05}(MA_{0.17}FA_{0.83})_{0.95}Pb(I_{0.83}Br_{0.17})_3$/PTAA/$NiO_x$/Au/PEN foil	NiO_x/Au/PEN foil	1.04	20.0	0.70	14.6	0.105	88% of PCE_i after 100 h at 80 °C	63

Table 1 (*continued*)

Configuration	Laminated electrode	V_{oc} (V)	J_{sc} (mA cm^{-2})	FF	PCE$_i$ (%)	Area (cm^2)	Stability	Ref.
ITO/SnO_2/$MAPbI_3$/Spiro-OMeTAD/sorbitol/PEDOT/ITO	Sorbitol/PEDOT/ITO	1.04	20.6	0.73	15.7	0.15	90% of PCE$_i$ after 100 h in 45% RH in the air	110
FTO/SnO_2/$CsFA_{0.83}MA_{0.17}PbI_{2.53}Br_{0.47}$/CuSCN/Carbon	Carbon film	1.09	21.1	0.66	15.3	0.115	93% of PCE$_i$ after 80 days in 55–70% RH	123
FTO/TiO_2 nanoparticles/$Cs_{0.17}FA_{0.83}Pb(I_{0.83}Br_{0.17})_3$/Spiro-OMeTAD/Carbon	Carbon film	0.98	18.3	0.70	12.2	0.04	80% of PCE$_i$ after 1000 h in the air	124
FTO/SnO_2/PCBM/$Cs_{0.05}(FA_{0.85}MA_{0.15})_{0.95}Pb(I_{0.85}Br_{0.15})_3$/Spiro-OMeTAD/composite carbon electrode	Carbon/conductive cloth film	1.1	22.2	0.80	19.3	0.1	N/A	126
ITO/PEN/SnO_2/PCBM/$Cs_{0.05}(FA_{0.85}MA_{0.15})_{0.95}Pb(I_{0.85}Br_{0.15})_3$/Spiro-OMeTAD/composite carbon electrode		1.05	20.3	0.72	15.3	0.1	89% of PCE$_i$ after 1176 bending cycles in air	
		1.09	20.0	0.64	14.0	1.0	66% of PCE$_i$ after 1240 bending cycles in the air	
FTO/c-TiO_2/m-TiO_2/$MAPbI_3$/Spiro-OMeTAD/PEDOT:PSS/D-sorbitol/Silver nanoparticle film/PET	PET/Ag nanoparticle film/PEDOT:PSS:D-sorbitol	0.97	18.0	0.59	10.5	1.0	15% of PCE$_i$ in 50% RH after 28 days	141
ITO/PEDOT:PSS/$FAPbI_{3-x}Br_x$/PCBM/PEDOT:PSS	PUA stamp/PEDOT:PSS (PH1000)	1.07	17.7	0.71	13.6	1.0	~90% of PCE$_i$ after 20 days in 30% RH	106
FTO/SnO_2/$(FA_{0.85}MA_{0.15})Pb(I_{0.85}Br_{0.15})_3$/Spiro-OMeTAD/Au-transfer	Au-transfer	1.06	21.4	0.76	17.1	0.16	N/A	85
ITO/PEDOT:PSS/$FAPbI_{3-x}Cl_x$/PCBM/PEI/AgNWs	PEI/AgNWs/OTS glass	0.97	18.5	0.71	12.7	N/A	N/A	142
Glass/SWCNT/$CuNiO_x$/KI/$Cs_{0.05}FA_{0.80}MA_{0.15}Pb(I_xBr_{1-x})_3$/choline chloride/PCBM/BCP/Ag	SWCNT films	1.12	21.4	0.78	19.0	0.09	80% of PCE$_i$ after 700 h in the air	134
PEN/SWCNT/$CuNiO_x$/KI/$Cs_{0.05}FA_{0.80}MA_{0.15}Pb(I_xBr_{1-x})_3$/choline chloride/PCBM/BCP/Ag		1.12	20.8	0.77	18.0			
PET/CuHC:dd PH1000/Cu:NiO_x/$MAPbI_3$/PC61BM/BCP/Cu	CuHC network	1.03	17.8	0.74	13.58	0.0725	90% of PCE$_i$ after 10 weeks in N_2	144

Spiro-OMeTAD = 2,2′,7,7′-tetrakis[*N*,*N*-di(4-methoxyphenyl)amino]-9,9′-spirobifluorene. TFSA = trifluoromethanesulfonic acid. PDMS = polydimethylsiloxane. TETA = triethylenetetramine. PTAA = poly[bis(4-phenyl)(2,4,6-trimethylphenyl)amine] or poly(triaryl)amine. PMMA = poly(methyl methacrylate).

an average PCE of 3.8%, significantly higher than that of the reported solar cells on CNC substrates with Ag electrode (PCE of 2.7%).[153,154]

Thermoplastic polymers such as PDMS and PET are extensively employed as transfer media in lamination methods.[77,153,155–157] To tackle the wettability problems of PDMS, an inexpensive plastic wrap was introduced as the alternative medium to transfer PEDOT:PSS as the top electrode for OPVs.[78,158] PEDOT:PSS-PH1000 coated on a plastic wrap could be easily transferred onto another stack without further wettability treatments, leading to the achievement of higher PCE of 4.0% compared to PCE of 3.5% for fabricated OPVs with PDMS.[78]

Utilizing PEDOT:PSS as the top electrode of organic tandem solar cells *via* the film-transfer lamination method was firstly reported by Tong *et al.*[159] They fabricated laminated tandem OPVs based on P3HT:ICBA as the active layer for both bottom and top cells with the stacked structure of glass/ITO/PEI/P3HT:ICBA/PH1000/PEI/P3HT:ICBA/PEDOT-T. After transferring the PEDOT:PSS/PDMS top electrode, the PDMS was peeled off from the laminated device. The tandem device showed a significant V_{oc} of 1.6 V, which is approximately the summation of the two individual sub-cells. PCEs of 2.5%, 3.0%, and 3.4% were obtained for the bottom and top sub-cells and the tandem structure, respectively. Also, the application of various lamination methods in tandem/ternary semitransparent OPVs with the polymer:dye:fullerene architecture has been reported by Makha *et al.* (Fig. 5c and d).[160] They coated PEDOT:PSS/D-sorbitol onto a flexible and transparent top electrode comprised of a PET/Ag mesh structure. The transparent top electrode was laminated onto the pre-fabricated cell stack at 120 °C by applying finger pressure. The laminated OPV with a 5 nm MoO_3 interlayer showed a PCE of 3.0%.

The solvent treatment method is proposed as an effective regular method to enhance the PEDOT:PSS layer conductivity.[161,162] However, this method suffers from challenges relating to the chemical and physical reactions of the substrates with strong acids (*i.e.*, H_3PO_4 and H_2SO_4),[161] raising the difficulty of washing the acid from the PEDOT:PSS matrix.

Therefore, Fan *et al.* developed a less destructive transfer-printing technology by employing a two-step sequential mild acid treatment including methanesulfonic acid (CH_4SO_3) dipping treatment and phosphoric acid (H_3PO_4) soaking treatment,[163] leading to enhanced conductivity of the flexible transparent electrode up to 3500 S cm^{-1}. The laminated flexible OPVs with the PEDOT:PSS/PEDOT:PSS (4083)/PBDTT-S-TT:$PC_{71}BM$/Ca/Al structure achieved PCEs of 5.38% and 4.8% for the mild acid-treated (CH_4SO_3 and H_3PO_4) and H_2SO_4-treated electrodes, respectively.

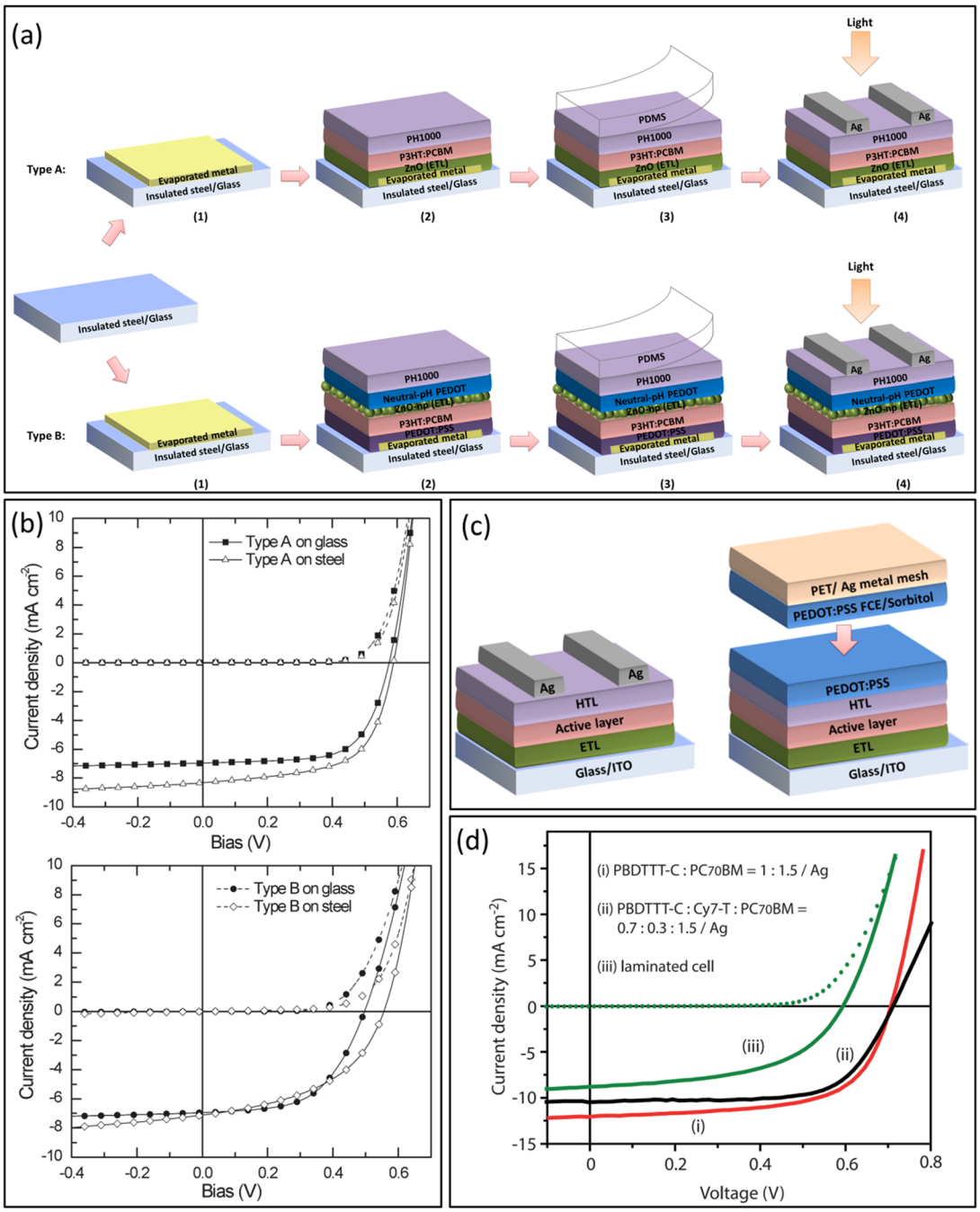

Fig. 5 (a) Schematic depiction of device fabrication steps for two different device types (A and B). (b) Dark current density–voltage (J–V) characteristic (dashed line) and under white light (AM1.5) illumination (solid lines) for Type A device and Type B device on glass with Cr (5 nm)/Au (100 nm) and insulated steel with Ag (100 nm) back contact [metal (100 nm)/ZnO (64 nm)/P3HT:PCBM (190 nm)/laminated PH1000 (120 nm)/Ag busbar (100 nm)], respectively. Reproduced with permission.[80] Copyright 2013, Wiley-VCH. (c) Schematic representation of the OPV with an evaporated silver (Ag) top electrode (left) and a transparent laminated electrode (right), (d) the related best J–V curves with TiO_2, PCDTTT-C/Cy7-T/PC70BM, and MoO_3 as ELT, active later, and HTL, respectively. Reproduced with permission.[160] Copyright 2017, Taylor & Francis.

Briefly, highly conductive PEDOT:PSS PH1000 (mainly with D-sorbitol) has been utilized in a majority of laminated OPVs. They were used in lamination methods with an e-glue to stick the top contact onto the device, as an electrode itself, or as a composite electrode being directly transferred onto the whole device stack using a transfer medium (mainly PDMS). In terms of performance, the highest PCEs reported for laminated OPVs using PH1000 as an e-glue and as a transfer-pressed electrode were 5.33% and 6.42%, respectively.[71,163]

3.2. Carbon materials for OPVs

As mentioned in the PSCs section, carbon materials, including SWCNTs, multi-walled carbon nanotube (MWCNT), graphene, and graphene oxide (GO), have been considered as the most

promising alternative bottom and top electrode candidates in OPVs as well.[81,164–167]

In this regard, Kim *et al.* transferred a transparent free-standing MWCNT (f-MWCNT) top electrode onto the n–i–p OPV device structure using a solution-assisted self-laminating process.[168] The as-prepared f-MWCNT sheets were manually deposited on top of the organic stacks, followed by immersion into an orthogonal liquid hydrofluoroether (HFE) solution to enhance the transparency and conductivity. As a result, PCEs of 1.5% and 0.9% for the bottom and top illumination were achieved, respectively. Also, the laminated f-MWCNT-based devices showed superior stability with PCE decay of only 3% after 700 h, while the device with Ag back contact showed 6% decay.

In a study of laminating CNTs, two transferring methods for the lamination of SWCNTs electrodes on top of OPVs were proposed, and two p-type dopants were also used as SWCNTs modifiers.[167] In the first method, SWCNT film was coated on the glass substrate, then doped with HNO_3 by drop-casting, and finally pressed onto the active layer using a UV resin as a transfer medium. In the second method, the SWCNT film was fixed on a metal holder, doped with MoO_x by thermal evaporation, and pressed onto the active layer.[167] The fabricated OPVs with two different lamination methods of HNO_3 and MoO_x-doped-SWCNTs exhibited PCEs of 3.7% and 3.1%, respectively. It was also implied that higher PCE up to 4.1% could be obtained with thicker SWCNT films but with lower transparency.

It should be considered that graphene sheets are competent candidates for laminated contact applications in OPVs.[169,170] Song *et al.* employed graphene as the anode or cathode and/or both the anode and cathode for the OPVs (Fig. 6a).[171] Graphene was synthesized on copper foil by a low-pressure CVD method, followed by depositing the polymeric layers of ethylene-vinyl-acetate (EVA) and PMMA. Afterward, the copper foil was removed to achieve a graphene/EVA/PMMA film. This film was scooped onto another piece of copper foil/graphene to produce a two-layer graphene film. The copper/two-layer graphene/EVA/PMMA stack was cut into small pieces and attached to the PDMS transfer medium. Then, the stack was annealed at 80 °C for 5 min, and PDMS was finally peeled off. As a result, flexible OPV devices with graphene as both the anode and cathode achieved a PCE of 3.8% with 61% device transparency. In a similar study, Tavakoli *et al.* laminated graphene/Cu/graphene foils between two EVA/PET substrates using a hot rolling process and modified the graphene quality by applying parylene as an interface layer on top of graphene (Fig. 6b).[172] The Cl-containing parylene reduced the damage during transfer by improving the adhesion to graphene and enhancing its conductivity. Then, they applied the two stacks of graphene/parylene/EVA/PET with sheet resistances of $<300\ \Omega\ sq^{-1}$ onto OPVs and achieved a PCE of 5.86% with the operational stability of over 30 days in ambient air. Also, Lee *et al.* fabricated semitransparent-inverted OPV devices with an alternative top electrode in the ITO/ZnO/P3HT:PCBM/GO/graphene architecture using a thermal release tape.[82] First, graphene film was synthesized on the copper foil, and then a thermal release tape was attached to the graphene film. The same process was repeated on the Cu foil to obtain optimal graphene layers. Then, the graphene film was transferred onto the cell at the GO interface, and the thermal release tape was removed. For eight graphene layers, a low sheet resistance of $\sim 100\ \Omega\ sq^{-1}$ was achieved, and the laminated OPV device showed a maximum PCE of 2.4% compared to the standard cell-based on Ag electrode with 3.30% PCE.

In short, from the optical transparency and electrical conductivity point of view for graphene- and CNT-based laminated electrodes in OPVs, both can be considered competitors of TCO electrodes ($>80\%$ transparency and $<40\ \Omega$ cm electrical resistance). However, the highest PCEs reported for the OPVs with laminated graphene as the bottom contact and CNTs as the top contact were 8.0% and 4.1%, respectively.[167,172]

3.3. Metal back contacts for OPVs

As mentioned earlier, the lamination method offers several advantages over metal evaporation. Highly conductive metallic top/bottom electrodes have also undergone the lamination methods rather than conventional vacuum-based methods, leading to enhanced PCE, improved stability, and avoiding the diffusion of the metal into the layers underneath in OPV devices. In this regard, Nakamura *et al.* deposited an Au electrode thermally on a glass substrate, followed by spin-coating a thin layer of PEDOT:PSS. Then, the glass/Au/PEDOT:PSS stack was laminated onto the ITO/TiO_2/P3HT:PCBM stack by a hydrostatic pressurizer at a pressure of 1 MPa and a temperature of 150 °C, achieving a PCE of 3.3%.[173] Similarly, Razali *et al.* investigated Au leaf as the top electrode for laminated OPVs based on P3HT:$PC_{61}BM$.[174] First, the Au leaf was coated on the PET substrate, and then it was transferred onto the solar cell at the interface of PEDOT:PSS. After which, a homogenous contact between the Au leaf and PEDOT:PSS was achieved under optimized lamination conditions, leading to a PCE of 2.8%. Moreover, the average PCE was increased to 5.07% when the $PC_{61}BM$ active layer was replaced with $PC_{71}BM$.

In addition, silver films are among the most common metal back contacts employed in the OPVs lamination process.[76,160,175,176] The fabrication of fully solution-processed OPV on the opaque substrate with laminated Ag-NWs films as the top anode was also reported by Gaynor *et al.*[149] To prepare the top transparent electrode, the Ag-NW suspension was drop-cast on a pre-cleaned glass, followed by annealing at 180 °C for 1 h. Then, the Ag-NW mesh films were pressed onto the device stack at a pressure of 5.9×10^3 psi (=40.68 MPa) for 30 s by a clean glass to compress the nanowire mesh, leading to the elimination of the undesired roughness and decreasing the sheet resistance. The ITO bottom substrate was also replaced with vacuum-deposited Ag film. As a result, the laminated OPV with the Ag/Cs_2CO_3/P3HT:PCBM/PEDOT:PSS/Ag nanowire structure achieved a PCE of 2.5%.

In brief, conventional lamination methods for the deposition of top/bottom electrodes and recent procedures to improve the performance of OPVs were reviewed. Depending on the contacts and CTLs, these methods include making an e-glue to

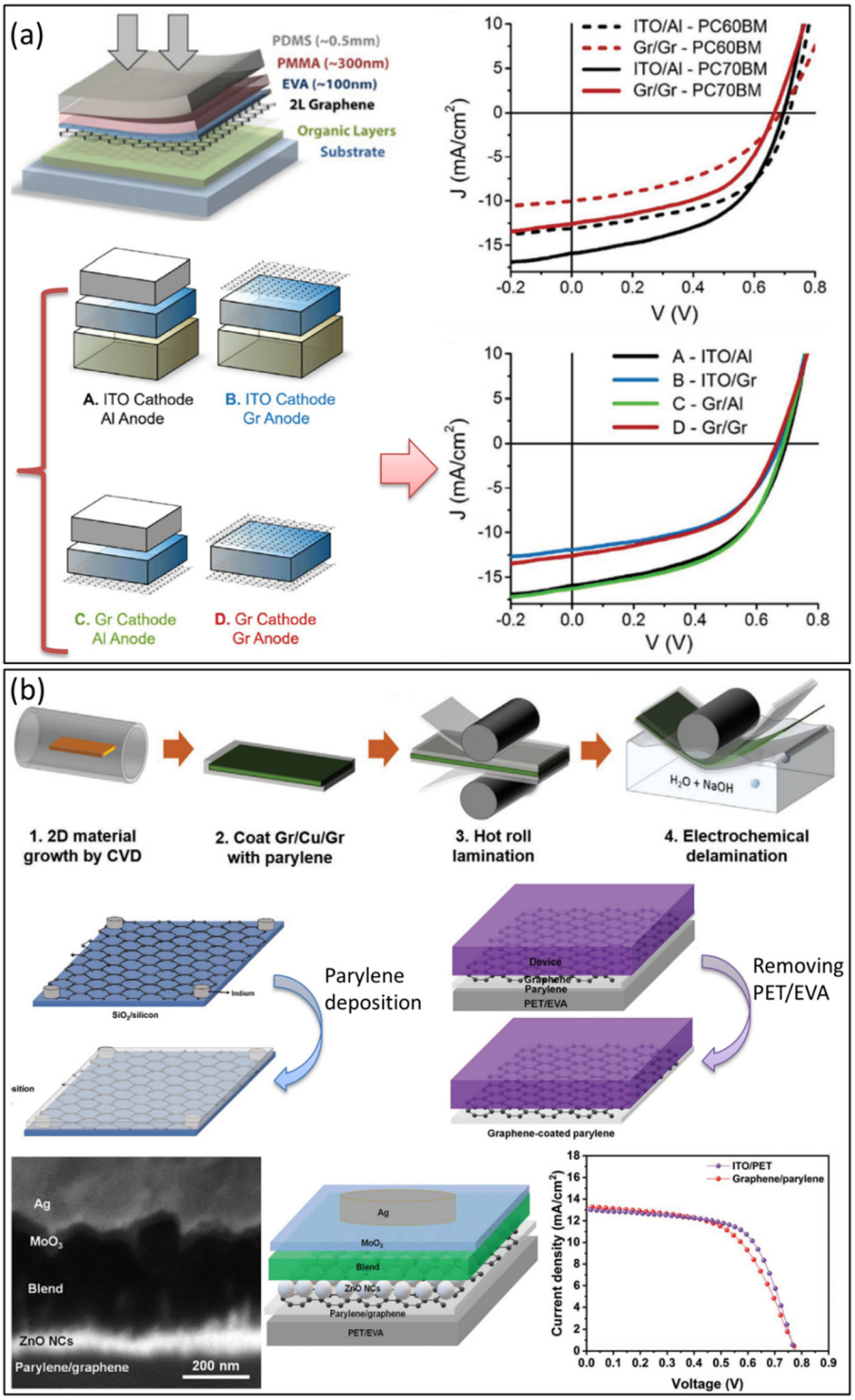

Fig. 6 (a) Schematic presentation of the stamp used for the dry-transfer of graphene top electrode. *J*–*V* curves of PSC devices based on Gr $PC_{60}BM$ and $PC_{70}BM$ on glass substrates (top row). Schematic illustration of different cathode and anode configurations. *J*–*V* curves of all device configurations for different cathodes and anodes based on $PC_{60}BM$ and $PC_{70}BM$ ETLs. Reproduced with permission.[171] Copyright 2016, Wiley-VCH. (b) Schematic representation of graphene growth in CVD furnace on both sides of Cu foil (orange) (top row). Schematics of graphene-coated SiO_2/silicon, before and after parylene deposition. Schematic of the OPV before and after removing the PET/EVA substrate (middle row). Schematic depiction of the OPV device fabricated on the graphene/parylene C (10 μm thick) using PV2000:$PC_{60}BM$ blend. *J*–*V* curves of the OPVs fabricated on ITO/PET and graphene/parylene C substrates (bottom row). Reproduced with permission.[172] Copyright 2020, Wiley-VCH.

stick the electrode onto the device, preparing free-standing carbon-based films and/or metal nanowires or nanoparticles on a substrate, and then pressing it onto the cell. The versatility of lamination methods could pave the way for the R2R

Table 2 The summarized device configuration, laminated electrodes, and photovoltaic characteristics of the laminated OPVs

Configuration	Laminated electrode	V_{oc} (V)	J_{sc} (mA cm^{-2})	FF	PCE$_i$ (%)	Active area (cm^2)	Stability	Ref.
ITO PET/Ag/MEH-PPV/C_{60}/Al	Ag	N/A	N/A	N/A	0.04	1	N/A	177
ITO/Cs_2CO_3/P3HT-PCBM blend/PED-OT:PSS:D-sorbitol/ITO	PEDOT:PSS:D-sorbitol/ITO	0.56	9.7	0.55	3.2	0.4	N/A	72
PEN/Ag/ZnO/P3HT:PC_{60}BM/PEDOT:PSS/Ag back contact	Ag back contact	N/A	N/A	N/A	2.3	4.8	N/A	175
ITO glass/c-TiO_2/P3HT:PC_{60}BM/Au	Au	0.60	9.9	0.54	3.3	0.03	N/A	173
Ag/Cs_2CO_3/P3HT:PC_{60}BM/PEDOT:PSS/Ag NW	Ag NW	0.51	10.6	0.46	2.5	0.02	N/A	149
ITO glass/ZnO/CuPc:C_{60}/BCP/Ag NW	Ag NW	0.44	1.9	0.55	0.6	0.01	N/A	178
ITO glass/Cs_2CO_3/P3HT:PC_{60}BM/PED-OT:PSS:D-sorbitol/Ag/PEN	PEDOT:PSS:D-sorbitol/Ag/PEN	0.59	10.7	0.63	4.0	N/A	N/A	148
ITO glass/ZnO/P3HT:PC_{60}BM/GO/Graphene	Graphene	0.54	10.5	0.44	2.5	0.1	N/A	82
AgNW/TiO_2/PEDOT:PSS/P3HT:PC_{60}BM/Ca/Al	Ag NW	0.56	9.5	0.63	3.4	0.01	N/A	179
ITO glass/doped-C_{60}/C_{60}/ZnPc:C_{60}/BF-DPB/MWCNTs	MWCNTs	0.57	4.7	0.58	1.5	0.69	N/A	168
ITO glass/PEDOT:PSS/PBDTT-DPP:PCBM/TiO_2/Ag NW/Al	Ag NW	0.77	9.3	0.56	4.0	0.1	N/A	180
PEN/Ag/Cs_2CO_3/P3HT:PCBM:$BaTiO_3$/PED-OT:PSS:D-sorbitol/Ag/PEN	PEDOT:PSS:D-sorbitol/Ag/PEN	0.53	11.4	0.64	3.8	N/A	Stable PCE at R = 4 mm	150
Wet-coated Ag/ZnO/P3HT:PCBM/PED-OT:PSS/Ag-grids	Wet-coated Ag	0.57	4.2	0.54	1.2	0.4	N/A	83
Type A: glass (Insulated steel)/Polyimide/Evaporated metal (Ag)/ZnO/P3HT:PCBM/PEDOT:PSS (PH1000)/Ag	PEDOT:PSS (PH1000)	0.59	8.3	0.61	3.2	0.09 and 0.16	N/A	80
Type B: Glass/insulated steel/polyimide/Ag/PEDOT:PSS/P3HT:PCBM/ZnO/PEDOT:PSS (neutral pH)/PEDOT:PSS (PH1000)/Ag	PEDOT:PSS (PH1000)	0.50	6.9	0.55	2.1		N/A	
ITO glass/ZnO/P3HT:PCBM/PEDOT:PSS/Ag	PEDOT: PSS/Ag	0.51	6.8	0.49	1.7 (average)	0.105	N/A	181
CNC/Ag/PEI/P3HT:ICBA/PEDOT:PSS (PH1000)	PEDOT:PSS (PH1000)	0.81	7.8	0.64	4.0	0.06	N/A	153
Graphene mesh/PEDOT:PSS/PSEHT-T:IC_{60}BA/PEDOT:PSS/PBDT-DPP:PC_{71}BM/	Ag Nanowire	1.62	7.6	0.64	8.02 (graphene)	0.04	N/A	182
TiO_2/Ag NW		1.62	6.7	0.6	6.47 (Ag NW)		N/A	
ITO glass/ZnO/P3HT:ICBA/PEDOT:PSS	PEDOT:PSS/plastic wrap	0.81	8.2	0.6	4.0 (average)	N/A	N/A	78
ITO glass/PEI/P3HT:ICBA/PH1000/PEI//P3HT:ICBA/PEDOT-T	PEDOT-T	1.62	3.2	0.72	3.6	0.05	N/A	159
PDMS/Transferred PEDOT:PSS flexible and transparent electrode (FTE)/PEDOT:PSS/PBDTT-S-TT:PC_{71}BM/Ca/Al	PDMS/PEDOT:PSS	0.82	14.2	0.55	6.4	0.06	83.4% of PCE$_i$ after 30 days in glovebox	163
PET/IMI/ZnO/PBTZT-*stat*-BDTT-8:PCBM/PEDOT:PSS:Sorbitol/Ag NWs/PET	PEDOT:PSS-Ag nanowire composite	0.81	12.1	0.59	5.8	0.15	N/A	71
ITO/ZnO/PTB7:PC_{71}BM:DIO/MoOx/SWNTs	SWNTs	0.7	9.0	0.65	4.1	0.09	N/A	167
PEN/PEDOT:PSS (PH1000)/PEDOT:PSS (AI4083)/PS NPs/PTB7:PC_{71}BM/TiO_x/Al	PEDOT:PSS (AI4083) + PS NPs/PUA stamp	0.74	14.7	0.52	5.7	0.09	65% of PCE$_i$ after 1000 bending cycles	183
Graphene on paper/PEDOT:PSS/ZnO/PDTP-DFBT:PCBM/MoO_3/graphene	PMMA/EVA/wo-layer graphene	0.68	9.8	0.43	2.8 (PC_{60}BM)	0.014	Stable PCE after 100 bending cycles at R = 1.2 mm	171
		0.67	12.4	0.45	3.7 (PC_{70}BM)			
ITO glass/c-TiO_2/PBDTTT-C:Cy7-T:PC_{70}BM/MoO_3/PEDOT:PSS HTL/PEDOT:PSS:Sorbitol/Ag mesh/PET	PEDOT:PSS:sorbitol/Ag mesh/PET	0.59	8.8	0.53	3.0	0.25	N/A	160
PET/EVA/parylene/graphene/ZnO nanoparticles (NCs)/PV2000:PC_{60}BM blend/MoO_3/Ag	Parylene/graphene	0.78	13.3	0.57	5.8	0.04	Stable PCE after 30 days in 40% RH	172
ITO glass/ZnO/PEIE/P3HT:PCBM/AgNW/PEDOT:PSS (PH1000)/NOA-63/EVA + PET	Glass/AgNW/EG-doped-PH1000/UV-curable adhesive/EVA/PET	0.61	8.1	0.53	2.6	0.04	N/A	184

MEH-PPV = poly[2-methoxy-5-(2′-ethylhexyloxy)-1,4-phenylene vinylene]. PBDTT-DPP = poly{2,6′-4,8-di(5 thylhexylthienyl)benzo[1,2-*b*;3,4-*b*]dithiophene-*alt*-5-dibutyloctyl-3,6-bis(5-bromothiophen-2-yl)-pyrrolo[3,4-*c*]pyrrole-1,4-dione}. ICBA = indene-C60 bisadduct, 1′,1″,4′,4″-tetrahydro-di[1,4]methanonaphthaleno[1,2 : 2′,3′,56,60 : 2″,3″][5,6]fullerene-C60. BF-DPB = *N*,*N*′-((diphenyl-*N*,*N*′-bis)9,9,-dimethyl-fluoren-2-yl)-benzidine. PET = polyethylene terephethalate. PEN = polyethylene naphthalate. PEI = polyethylene imine. CNC = cellulose nanocrystal. BCP = bathocuproine. P3HT = poly(3-hexylthiophene-2,5-diyl). PCBM = Phenyl-C60-butyric acid methyl ester. PC71BM = poly(5,10-bis(5-(thiophen-2-yl)-4-(2-decyltetradecyl)thiophen-2-yl)-naphtho[1,2-*c*:5,6-*cA*]bis[1,2,5]thiadiazole) (PNTz4T):[6,6]phenyl-C71-butyric acid methyl ester.

Table 3 The comparison of lamination means, advantages, and challenges of the laminate material layers

PEDOT:PSS film		Ref.
Lamination applications	Mixed with additives such as e-glue As a TCA in sandwich structures As a free-standing film As a composite electrode with metal(carbon) grids using a transfer medium	94, 95, 101, 106, 110 and 183
Advantages	High optical transparency Appropriate work function Superb hole transport behavior High conductivity (Clevios PH1000) Good flexibility Adaptable to a majority of coating methods Applicable for R2R methods and tandem structures	
Challenges	Low conductivity of PSS fraction Requires a dopant (*i.e.*, D-sorbitol) Hydrophilic nature and extreme tendency to absorb water Requiring O_2/UVO treatment before coating	
Carbon film		
Lamination application	Solvent exchange of the carbon pastes to use as free-standing carbon films Free-standing CVD-produced CNT films As a composite electrode used in dry-transfer methods	65, 122, 123, 127, 128, 133, 171 and 172
Advantages	Reduced costs Chemical inertness Suitable work function High mechanical flexibility High conductivity Hydrophobic nature Enabling the R2R deposition process	
Challenges	Requiring a conductivity enhancer Increasing the cell temperature inside PSCs Requiring an HTL for high PCEs	
Inorganic film		
Lamination application	As a metal foil to stack on the cell As a metal film to be transferred *via* transfer mediums	85, 143 and 173
Advantages	The highest conductivity and lowest sheet resistance Desired work function	
Challenges	High costs Degrading the interface with perovskite in PSCs Hard to obtain a uniform film	

production of semitransparent and tandem OPVs on flexible substrates with various device configurations.

The summarized device configuration, laminated electrodes, and photovoltaic characteristics of the lamination-produced OPVs in the literature are reviewed in Table 2.

The comparative view of the transport layers applied in lamination methods reviewed herein is presented in Table 3. The most remarkable lamination methods for the deposition of CTLs and/or bottom/top contacts to substitute the vacuum-based deposition of high-cost Au or rigid ITO glass in the PSC architecture were reviewed. The dry transfer-based methods (mainly dry stamp transfer) are the mainstream among the various lamination methods employed. This is because they enable the direct deposition of electrodes without damaging other moisture-sensitive layers within the devices. As a result, these methods could employ a broader range of materials. However, they require annealing, high temperature before applying, and a medium for sticking to the device stack. The e-glue-based lamination, as another major method, needs no further temperature during the process. Still, its components (mainly PH1000 and sorbitol) endanger the device's stability and performance in the long run. This review classified the most commonly employed laminate materials as PEDOT:PSS (PH1000) composites, various carbon films, and inorganic (metal) films. In each section, the mechanism and strategies for applying the deposition of electrodes using lamination methods in the literature about the specific PSC structure were briefly represented. One should consider the Fermi energy level alignment with perovskite or HTL, electrical conductivity, stability issues, ohmic interfacial resistance, and interfacial interactions between perovskite and HTL under high temperature and pressure when applying the lamination materials, and methods thereof in PSCs. Therefore, these methods primarily impact the FF of the devices if the laminated contact showed low conductivity and high series resistance. Also, ultrahigh pressure and destructive materials to the sensitive perovskite film would damage the current density and charge extraction at the interfaces. These could be the major challenges affecting the PCE and stability of the lamination-produced devices, which should be addressed to further boost their performance.

4. Conclusion and outlook

Lamination methods were introduced as one of the most promising methods for fabricating large-scale PSC and OPV

devices to overcome the limitation of the standard thermal evaporation metal electrodes, *i.e.*, Ag and Au. The lamination methods enable the production of cost-effective, easy-to-fabricate, self-encapsulated, and processable in ambient conditions solar cells and chemically inert electrodes to replace evaporated metal electrodes. These methods include the deposition of different thin films, and the majority of them focus on the top/bottom electrode.

This review discussed three well-known lamination electrodes based on PEDOT:PSS, carbon films, and metal back contacts for PSCs and OPVs. The performances of PSCs still lag behind the certified record of PSCs based on thermally-evaporated contacts by almost 5% in both small-scale and solar modules. This might have been due to the imperfect contact between the laminated electrodes and the device stack, leading to the poor electrical connection at the interfaces during the inserted pressure. However, the laminated PSCs achieved more success than their OPVs counterpart, reaching the best PCEs of 15.7%, 19.3%, and 17.4% for PEDOT:PSS, carbon films, and Au-laminated electrodes, respectively. Moreover, the carbon films have shown remarkable potential as a laminated electrode to fabricate highly efficient PSCs. On the other side, laminated OPVs achieved record PCEs of 5.3%, 6.2%, 8.0%, 4.1%, and 5.0% for PH1000 (PEDOT:PSS/D-sorbitol) as an e-glue electrode, PH1000 as a transfer-pressed electrode, graphene as the bottom contact, CNT as the top contact, and Au leaf as the top contact, respectively. Overall, CNTs, as a family of carbon films, have great potential within highly efficient OPVs.

Different parts of a device can be laminated to fabricate PSCs and OPVs. For example, in the PSCs section, we discussed the lamination of two different half-stacks from perovskite/perovskite interface deposited on separate substrates or wet pre-deposited HTL/perovskite interface, *i.e.*, sandwich structure, laminating the polymeric top electrodes, carbon films, and metal back electrodes. For laminating the polymeric top electrodes (usually PEDOT:PSS/adhesive), it is typically coated on the transfer medium (PDMS, plastic wrap, glass, *etc.*) and then laminated on the second stack to solve the wettability challenge of the polymeric film during device fabrication. On the other hand, in the OPVs section, we also focused on laminating the photoactive polymer layer and the anode or cathode stacks. The commercialization of PSC and OPV devices is moving fast, opening the door for R2R production on flexible substrates and tandem structures.

Conflicts of interest

The authors declare no conflict of interest.

Acknowledgements

M. S. thanks the German Research Foundation (DFG) for funding (SPP2196, 431314977/GRK 2642). M. S. acknowledges funding by ProperPhotoMile. Project ProperPhotoMile is supported under the umbrella of SOLAR-ERA.NET Cofund 2 by The Spanish Ministry of Science and Education and the AEI under the project PCI2020-112185 and CDTI project number IDI-20210171; the Federal Ministry for Economic Affairs and Energy on the basis of a decision by the German Bundestag project number FKZ 03EE1070B and FKZ 03EE1070A and the Israel Ministry of Energy with project number 220-11-031. SOLAR-ERA.NET is supported by the European Commission within the EU Framework Programme for Research and Innovation HORIZON 2020 (Cofund ERA-NET Action, No. 786483).

References

1 M. Malekshahi Byranvand, A. Nemati Kharat, N. Taghavinia and A. Dabirian, *ACS Appl. Mater. Interfaces*, 2016, **8**, 16359–16367.
2 Z. Hosseini, N. Taghavinia and E. W. G. Diau, *Mater. Lett.*, 2017, **188**, 92–94.
3 M. J. Berry, *Nature*, 1991, **354**, 737–740.
4 A. Dabirian, M. M. Byranvand, A. Naqavi, A. N. Kharat and N. Taghavinia, *ACS Appl. Mater. Interfaces*, 2016, **8**, 247–255.
5 M. M. Byranvand, N. Taghavinia, A. N. Kharat and A. Dabirian, *RSC Adv.*, 2015, **5**, 86050–86055.
6 M. M. Byranvand, A. Dabirian, A. N. Kharat and N. Taghavinia, *RSC Adv.*, 2015, **5**, 33098–33104.
7 S. Arabzade, M. Samadpour and N. Taghavinia, *RSC Adv.*, 2015, **5**, 45592–45598.
8 M. Tavakkoli, R. Ajeian, M. Nakhaee Badrabadi, S. Saleh Ardestani, S. M. H. Feiz and K. Elahi Nasab, *Sol. Energy Mater. Sol. Cells*, 2011, **95**, 1964–1969.
9 M. Nakhaee Badrabadi, R. Ajeian, S. Saleh Ardestani and M. Tavakkoli, *Org. Electron.*, 2012, **13**, 2682–2687.
10 S. Saleh Ardestani, R. Ajeian, M. Nakhaee Badrabadi and M. Tavakkoli, *Sol. Energy Mater. Sol. Cells*, 2013, **111**, 107–111.
11 F. Obeidat, *Sol. Energy*, 2018, **163**, 545–551.
12 Z. Saki, K. Aitola, K. Sveinbjörnsson, W. Yang, S. Svanström, U. B. Cappel, H. Rensmo, E. M. J. Johansson, N. Taghavinia and G. Boschloo, *J. Power Sources*, 2018, **405**, 70–79.
13 Z. Saki, K. Sveinbjörnsson, G. Boschloo and N. Taghavinia, *ChemPhysChem*, 2019, **20**, 3322–3327.
14 Z. Saki, M. M. Byranvand, N. Taghavinia, M. Kedia and M. Saliba, *Energy Environ. Sci.*, 2021, **14**(11), 5690–5722.
15 K. Sveinbjörnsson, N. K. Kyi Thein, Z. Saki, S. Svanström, W. Yang, U. B. Cappel, H. Rensmo, G. Boschloo, K. Aitola and E. M. J. Johansson, *Sustainable Energy Fuels*, 2018, **2**, 606–615.
16 A. Hultqvist, K. Aitola, K. Sveinbjörnsson, Z. Saki, F. Larsson, T. Törndahl, E. Johansson, G. Boschloo and M. Edoff, *ACS Appl. Mater. Interfaces*, 2017, **9**, 29707–29716.
17 M. Samadpour, A. Golchini, K. Abdizadeh, M. Heydari, M. Forouzandeh, Z. Saki and N. Taghavinia, *ACS Omega*, 2021, **6**, 172–179.
18 L. Schmidt-Mende, V. Dyakonov, S. Olthof, F. Ünlü, K. M. T. Lê, S. Mathur, A. D. Karabanov, D. C. Lupascu, L. M. Herz, A. Hinderhofer, F. Schreiber, A. Chernikov,

D. A. Egger, O. Shargaieva, C. Cocchi, E. Unger, M. Saliba, M. M. Byranvand, M. Kroll, F. Nehm, K. Leo, A. Redinger, J. Höcker, T. Kirchartz, J. Warby, E. Gutierrez-Partida, D. Neher, M. Stolterfoht, U. Würfel, M. Unmüssig, J. Herterich, C. Baretzky, J. Mohanraj, M. Thelakkat, C. Maheu, W. Jaegermann, T. Mayer, J. Rieger, T. Fauster, D. Niesner, F. Yang, S. Albrecht, T. Riedl, A. Fakharuddin, M. Vasilopoulou, Y. Vaynzof, D. Moia, J. Maier, M. Franckevičius, V. Gulbinas, R. A. Kerner, L. Zhao, B. P. Rand, N. Glück, T. Bein, F. Matteocci, L. A. Castriotta, A. Di Carlo, M. Scheffler and C. Draxl, *APL Mater.*, 2021, **9**, 109202.

19 H. Liu, M. H. Yu, C. C. Lee, X. Yu, Y. Li, Z. Zhu, C. C. Chueh, Z. Li and A. K. Y. Jen, *Adv. Mater. Technol.*, 2021, **6**, 2000960.

20 S. K. Sahoo, B. Manoharan and N. Sivakumar, *Perovskite Photovoltaics*, 2018, 1–24, DOI: **10.1016/B978-0-12-812915-9.00001-0**.

21 K. Fukuda, K. Yu and T. Someya, *Adv. Energy Mater.*, 2020, **10**, 2000765.

22 J. Huang, Z. Ren, Y. Zhang, K. Liu, H. Zhang, H. Tang, C. Yan, Z. Zheng and G. Li, *Adv. Funct. Mater.*, 2021, **31**, 2010172.

23 R. Rafiei Rad, B. Azizollah Ganji and N. Taghavinia, *Opt. Mater.*, 2022, **123**, 111876.

24 A. Kojima, K. Teshima, Y. Shirai and T. Miyasaka, *J. Am. Chem. Soc.*, 2009, **131**, 6050–6051.

25 J. J. Yoo, G. Seo, M. R. Chua, T. G. Park, Y. Lu, F. Rotermund, Y. K. Kim, C. S. Moon, N. J. Jeon, J. P. Correa-Baena, V. Bulović, S. S. Shin, M. G. Bawendi and J. Seo, *Nature*, 2021, **590**, 587–593.

26 K. Minjin, J. Jaeki, L. Haizhou, L. T. Kyung, E. F. T. Eickemeyer, L. Yuhang, C. I. Woo, C. S. Ju, J. Yimhyun, K. Hak-Beom, M. Sung-In, K. Young-Ki, L. Heunjeong, A. N. Gyeong, C. Shinuk, T. W. R. Tress, Z. S. M. Zakeeruddin, H. Anders, K. J. Young, G. Michael and K. D. Suk, *Science*, 2022, **375**(6578), 302–306.

27 S. E. Shaheen, C. J. Brabec, N. S. Sariciftci, F. Padinger, T. Fromherz and J. C. Hummelen, *Appl. Phys. Lett.*, 2001, **78**, 841–843.

28 L. Wang, Q. An, L. Yan, H.-R. Bai, M. Jiang, A. Mahmood, C. Yang, H. Zhi and J.-L. Wang, *Energy Environ. Sci.*, 2022, **15**, 320–333.

29 Best Research-Cell Efficiency Chart, **https://www.nrel.gov/pv/cell-efficiency.html**.

30 G. Yang, Z. Ren, K. Liu, M. Qin, W. Deng, H. Zhang, H. Wang, J. Liang, F. Ye, Q. Liang, H. Yin, Y. Chen, Y. Zhuang, S. Li, B. Gao, J. Wang, T. Shi, X. Wang, X. Lu, H. Wu, J. Hou, D. Lei, S. K. So, Y. Yang, G. Fang and G. Li, *Nat. Photonics*, 2021, **15**, 681–689.

31 I. Mesquita, L. Andrade and A. Mendes, *Renewable Sustainable Energy Rev.*, 2018, **82**, 2471–2489.

32 M. Heidariramsheh, M. Mirhosseini, K. Abdizadeh, S. M. Mahdavi and N. Taghavinia, *ACS Appl. Energy Mater.*, 2021, **4**, 5560–5573.

33 M. M. Byranvand, T. Kim, S. Song, G. Kang, S. U. Ryu and T. Park, *Adv. Energy Mater.*, 2018, **8**, 1702235.

34 J. Lee, M. Malekshahi Byranvand, G. Kang, S. Y. Son, S. Song, G. W. Kim and T. Park, *J. Am. Chem. Soc.*, 2017, **139**, 12175–12181.

35 M. Seri, F. Mercuri, G. Ruani, Y. Feng, M. Li, Z. X. Xu and M. Muccini, *Energy Technol.*, 2021, **9**, 2000901.

36 M. A. Alkhalayfeh, A. A. Aziz and M. Z. Pakhuruddin, *Renewable Sustainable Energy Rev.*, 2021, **141**, 110726.

37 E. H. Jung, N. J. Jeon, E. Y. Park, C. S. Moon, T. J. Shin, T. Y. Yang, J. H. Noh and J. Seo, *Nature*, 2019, **567**, 511–515.

38 Y. Wei, J. Yu, L. Qin, H. Chen, X. Wu, Z. Wei, X. Zhang, Z. Xiao, L. Ding, F. Gao and H. Huang, *Energy Environ. Sci.*, 2021, **14**, 2314–2321.

39 X. Li, X. Du, J. Zhao, H. Lin, C. Zheng and S. Tao, *Sol. RRL*, 2021, **5**, 2000592.

40 Y. Vaynzof, *Adv. Energy Mater.*, 2020, **10**, 2003073.

41 M. R. Samantaray, N. K. Rana, A. Kumar, D. S. Ghosh and N. Chander, *Int. J. Energy Res.*, 2021, **46**, 1250–1262.

42 H. K. Kim, K. B. Chung and J. Kal, *J. Alloys Compd.*, 2019, **778**, 487–495.

43 S. Han, Y. Deng, W. Han, G. Ren, Z. Song, C. Liu and W. Guo, *Sol. Energy*, 2021, **225**, 97–107.

44 K. Domanski, J. P. Correa-Baena, N. Mine, M. K. Nazeeruddin, A. Abate, M. Saliba, W. Tress, A. Hagfeldt and M. Grätzel, *ACS Nano*, 2016, **10**, 6306–6314.

45 Y. Rong, Y. Hu, A. Mei, H. Tan, M. I. Saidaminov, S. Il Seok, M. D. McGehee, E. H. Sargent and H. Han, *Science*, 2018, **361**, eaat8235.

46 M. Riede, D. Spoltore and K. Leo, *Adv. Energy Mater.*, 2021, **11**, 2002653.

47 T. Leijtens, G. E. Eperon, S. Pathak, A. Abate, M. M. Lee and H. J. Snaith, *Nat. Commun.*, 2013, **4**, 2885.

48 X. Tian, S. D. Stranks and F. You, *Nat. Sustainability*, 2021, **4**, 821–829.

49 G. Grancini, C. Roldán-Carmona, I. Zimmermann, E. Mosconi, X. Lee, D. Martineau, S. Narbey, F. Oswald, F. De Angelis, M. Graetzel and M. K. Nazeeruddin, *Nat. Commun.*, 2017, **8**, 15684.

50 M. Que, B. Zhang, J. Chen, X. Yin and S. Yun, *Mater. Adv.*, 2021, **2**, 5560–5579.

51 Q. Luo, R. Wu, L. Ma, C. Wang, H. Liu, H. Lin, N. Wang, Y. Chen and Z. Guo, *Adv. Funct. Mater.*, 2020, **31**, 2004765.

52 L. Wieland, H. Li, C. Rust, J. Chen and B. S. Flavel, *Adv. Energy Mater.*, 2021, **11**, 2002880.

53 G. R. Li and X. P. Gao, *Adv. Mater.*, 2020, **32**, 1806478.

54 S. P. Dunfield, D. T. Moore, T. R. Klein, D. M. Fabian, J. A. Christians, A. G. Dixon, B. Dou, S. Ardo, M. C. Beard, S. E. Shaheen, J. J. Berry and M. F. A. M. Van Hest, *ACS Energy Lett.*, 2018, **3**, 1192–1197.

55 B. Yang, Y. Xie, P. Zeng, Y. Dong, Q. Ou and S. Zhang, *Appl. Sci.*, 2020, **10**, 1917.

56 J. H. Heo, H. J. Han, M. Lee, M. Song, D. H. Kim and S. H. Im, *Energy Environ. Sci.*, 2015, **8**, 2922–2927.

57 N. Ahn, I. Jeon, J. Yoon, E. I. Kauppinen, Y. Matsuo, S. Maruyama and M. Choi, *J. Mater. Chem. A*, 2018, **6**, 1382–1389.

58 Z. Li, S. A. Kulkarni, P. P. Boix, E. Shi, A. Cao, K. Fu, S. K. Batabyal, J. Zhang, Q. Xiong, L. H. Wong, N. Mathews and S. G. Mhaisalkar, *ACS Nano*, 2014, **8**, 6797–6804.
59 S. S. Shin, E. J. Yeom, W. S. Yang, S. Hur, M. G. Kim, J. Im, J. Seo, J. H. Noh and S. Il Seok, *Science*, 2017, **356**, 167–171.
60 Y. Xiao, G. Han, H. Zhou and J. Wu, *RSC Adv.*, 2016, **6**, 2778–2784.
61 J. Ouyang and Y. Yang, *Adv. Mater.*, 2006, **18**, 2141–2144.
62 M. Makha, S. L. Fernandes, S. Jenatsch, T. Offermans, J. Schleuniger, J.-N. N. Tisserant, A. C. Véron and R. Hany, *Sci. Technol. Adv. Mater.*, 2016, **17**, 260–266.
63 R. Schmager, J. Roger, J. A. Schwenzer, F. Schackmar, T. Abzieher, M. Malekshahi Byranvand, B. Abdollahi Nejand, M. Worgull, B. S. Richards and U. W. Paetzold, *Adv. Funct. Mater.*, 2020, **30**, 1907481.
64 Y. Shao, C. Zhang, S. Wang, Y. Yan, Y. Feng, J. Bian and Y. Shi, *Adv. Mater. Interfaces*, 2019, **6**, 1900157.
65 C. W. Jang, J. M. Kim and S. H. Choi, *J. Alloys Compd.*, 2019, **775**, 905–911.
66 W. A. Dunlap-Shohl, Y. Zhou, N. P. Padture and D. B. Mitzi, *Chem. Rev.*, 2019, **119**, 3193–3295.
67 M. M. Byranvand, C. Otero-Martínez, J. Ye, W. Zuo, L. Manna, M. Saliba, R. L. Z. Hoye and L. Polavarapu, *Adv. Opt. Mater.*, 2022, **10**, 2200423.
68 J. Roger, L. K. Schorn, M. Heydarian, A. Farag, T. Feeney, D. Baumann, H. Hu, F. Laufer, W. Duan, K. Ding, A. Lambertz, P. Fassl, M. Worgull and U. W. Paetzold, *Adv. Energy Mater.*, 2022, **12**, 2200961.
69 M. M. Byranvand, T. Kodalle, W. Zuo, T. Magorian Friedlmeier, M. Abdelsamie, K. Hong, W. Zia, S. Perween, O. Clemens, C. M. Sutter-Fella and M. Saliba, *Adv. Sci.*, 2022, DOI: **10.1002/advs.202202441**.
70 C. Shimada and S. Shiratori, *ACS Appl. Mater. Interfaces*, 2013, **5**, 11087–11092.
71 G. D. Spyropoulos, C. O. Ramirez Quiroz, M. Salvador, Y. Hou, N. Gasparini, P. Schweizer, J. Adams, P. Kubis, N. Li, E. Spiecker, T. Ameri, H. J. Egelhaaf and C. J. Brabec, *Energy Environ. Sci.*, 2016, **9**, 2302–2313.
72 J. Huang, G. Li and Y. Yang, *Adv. Mater.*, 2008, **20**, 415–419.
73 Y. Xia, X. Xu, L. E. Aguirre and O. Inganäs, *J. Mater. Chem. A*, 2018, **6**, 21186–21192.
74 J. Bergqvist, T. Österberg, A. Melianas, L. Ever Aguirre, Z. Tang, W. Cai, Z. Ma, M. Kemerink, D. Gedefaw, M. R. Andersson and O. Inganäs, *npj Flexible Electron.*, 2018, **2**, 1–8.
75 D. Kaduwal, B. Zimmermann and U. Würfel, *Sol. Energy Mater. Sol. Cells*, 2014, **120**, 449–453.
76 Z. Lin, W. Guan, W. Cai, L. Wang, X. Wang, Z. He and L. Hou, *Energy Sci. Eng.*, 2021, **9**, 502–508.
77 F. Jiang, T. Liu, S. Zeng, Q. Zhao, X. Min, Z. Li, J. Tong, W. Meng, S. Xiong and Y. Zhou, *Opt. Express*, 2015, **23**, A83–A91.
78 L. Yin, Z. Zhao, F. Jiang, Z. Li, S. Xiong and Y. Zhou, *Org. Electron.*, 2014, **15**, 2593–2598.
79 X. Li, X. Tang, T. Ye, D. Wu, H. Wang and X. Wang, *ACS Appl. Mater. Interfaces*, 2017, **9**, 18730–18738.
80 D. Gupta, M. M. Wienk and R. A. J. Janssen, *Adv. Energy Mater.*, 2013, **3**, 782–787.
81 K. T. Lee, D. H. Park, H. W. Baac and S. Han, *Materials*, 2018, **11**, 1503.
82 Y.-Y. Lee, K.-H. Tu, C.-C. Yu, S.-S. Li, J.-Y. Hwang, C.-C. Lin, K.-H. Chen, L.-C. Chen, H.-L. Chen and C.-W. Chen, *ACS Nano*, 2011, **5**, 6564–6570.
83 Y. M. Chang, C. P. Chen, J. M. Ding, C. Y. Leu, M. J. Lee and R. De Chen, *Sol. Energy Mater. Sol. Cells*, 2013, **109**, 91–96.
84 L. Bu, Z. Liu, M. Zhang, W. Li, A. Zhu, F. Cai, Z. Zhao and Y. Zhou, *ACS Appl. Mater. Interfaces*, 2015, **7**, 17776–17781.
85 Q. Li, J. Xiao, C. Peng, Q. Duan, Z. Ku, J. Zhong, W. Li, Y. Peng, F. Huang and Y. B. Cheng, *Mater. Lett.*, 2021, **301**, 130244.
86 B. Abdollahi Nejand, S. Gharibzadeh, V. Ahmadi and H. R. Shahverdi, *J. Phys. Chem. C*, 2016, **120**, 2520–2528.
87 N. Cheng, P. Liu, F. Qi, Y. Xiao, W. Yu, Z. Yu, W. Liu, S. S. Guo and X. Z. Zhao, *J. Power Sources*, 2016, **332**, 24–29.
88 J. H. Heo, D. H. Shin, M. L. Lee, M. G. Kang and S. H. Im, *ACS Appl. Mater. Interfaces*, 2018, **10**, 31413–31421.
89 C. C. Boyd, R. Cheacharoen, T. Leijtens and M. D. McGehee, *Chem. Rev.*, 2019, **119**, 3418–3451.
90 W. A. Dunlap-Shohl, T. Li and D. B. Mitzi, *ACS Appl. Energy Mater.*, 2019, **2**, 5083–5093.
91 Y. Jiang, B. Luo, F. Jiang, F. Jiang, C. Fuentes-Hernandez, T. Liu, L. Mao, S. Xiong, Z. Li, T. Wang, B. Kippelen and Y. Zhou, *Nano Lett.*, 2016, **16**, 7829–7835.
92 L. Hu, M. Li, K. Yang, Z. Xiong, B. Yang, M. Wang, X. Tang, Z. Zang, X. Liu, B. Li, Z. Xiao, S. Lu, H. Gong, J. Ouyang and K. Sun, *J. Mater. Chem. A*, 2018, **6**, 16583–16589.
93 J. Niu, D. Yang, X. Ren, Z. Yang, Y. Liu, X. Zhu, W. Zhao and S. (Frank) Liu, *Org. Electron.*, 2017, **48**, 165–171.
94 K. M. Reza, A. Gurung, B. Bahrami, S. Mabrouk, H. Elbohy, R. Pathak, K. Chen, A. H. Chowdhury, M. T. Rahman, S. Letourneau, H. C. Yang, G. Saianand, J. W. Elam, S. B. Darling and Q. Qiao, *J. Energy Chem.*, 2020, **44**, 41–50.
95 K. M. Reza, S. Mabrouk and Q. Qiao, *Proc. Nat. Res. Soc.*, 2018, **2**, 02004.
96 L. Xu, Y. Li, C. Zhang, Y. Liu, C. Zheng, W. Z. Lv, M. Li, Y. Chen, W. Huang and R. Chen, *Sol. Energy Mater. Sol. Cells*, 2020, **206**, 110316.
97 N. Espinosa, R. García-Valverde, A. Urbina and F. C. Krebs, *Sol. Energy Mater. Sol. Cells*, 2011, **95**, 1293–1302.
98 Z. Zhou and M. Carbajales-Dale, *Energy Environ. Sci.*, 2018, **11**, 603–608.
99 Y. Cui, G. Jia, J. Zhu, Q. Kang, H. Yao, L. Lu, B. Xu and J. Hou, *Chem. Mater.*, 2018, **30**, 1078–1084.
100 D. Bryant, P. Greenwood, J. Troughton, M. Wijdekop, M. Carnie, M. Davies, K. Wojciechowski, H. J. Snaith, T. Watson and D. Worsley, *Adv. Mater.*, 2014, **26**, 7499–7504.
101 D. A. W. Worsley, T. M. W. Joel Troughton, D. Bryant, K. Wojciechowski, M. J. Carnie and H. Snaith, *J. Mater. Chem. C*, 2015, **3**, 10715–10722.
102 L. Hu, J. Song, X. Yin, Z. Su and Z. Li, *Polymers*, 2020, **12**, 145.

103 X. Hu, X. Meng, L. Zhang, Y. Zhang, Z. Cai, Z. Huang, M. Su, Y. Wang, M. Li, F. Li, X. Yao, F. Wang, W. Ma, Y. Chen and Y. Song, *Joule*, 2019, **3**, 2205–2218.
104 H. Zhang, Y. Zhang, G. Yang, Z. Ren, W. Yu, D. Shen, C. S. Lee, Z. Zheng and G. Li, *Sci. China: Chem.*, 2019, **62**, 875–882.
105 L. Liang, Y. Cai, X. Li, M. K. Nazeeruddin and P. Gao, *Nano Energy*, 2018, **52**, 211–238.
106 J. H. Lee, J. H. Heo, S. H. Im and O. O. Park, *ACS Appl. Mater. Interfaces*, 2020, **12**, 10527–10534.
107 M. Mohammadi, S. Gholipour, M. Malekshahi Byranvand, Y. Abdi, N. Taghavinia and M. Saliba, *ACS Appl. Mater. Interfaces*, 2021, **13**, 45455–45464.
108 R. K. Raman, S. A. Gurusamy Thangavelu, S. Venkataraj and A. Krishnamoorthy, *Renewable Sustainable Energy Rev.*, 2021, **151**, 111608.
109 S. I. Cha, Y. Kim, K. H. Hwang, Y. J. Shin, S. H. Seo and D. Y. Lee, *Energy Environ. Sci.*, 2012, **5**, 6071–6075.
110 T. Li, W. A. Dunlap-Shohl and D. B. Mitzi, *ACS Appl. Energy Mater.*, 2020, **3**, 9493–9497.
111 C. Zhou and S. Lin, *Sol. RRL*, 2020, **4**, 1900190.
112 R. He, X. Huang, M. Chee, F. Hao and P. Dong, *Carbon Energy*, 2019, **1**, 109–123.
113 H. Zhang, K. Song, L. Zhu and Q. Meng, *Carbon*, 2020, **168**, 372–391.
114 H. Su, T. Wu, D. Cui, X. Lin, X. Luo, Y. Wang and L. Han, *Small Methods*, 2020, **4**, 2000507.
115 X. Chang, W. Li, H. Chen, L. Zhu, H. Liu, H. Geng, S. Xiang, J. Liu, X. Zheng, Y. Yang and S. Yang, *ACS Appl. Mater. Interfaces*, 2016, **8**, 30184–30192.
116 H. N. Chen, Z. H. Wei, H. X. He, X. L. Zheng, K. S. Wong and S. H. Yang, *Adv. Energy Mater.*, 2016, **6**, 1502087.
117 S. Zhu, J. Tian, J. Zhang, C. Gao and X. Liu, *ACS Appl. Energy Mater.*, 2021, **4**, 5554–5559.
118 M. Tian, C. Y. Woo, J. W. Choi, J. Y. Seo, J. M. Kim, S. H. Kim, M. Song and H. W. Lee, *ACS Appl. Mater. Interfaces*, 2020, **12**, 54806–54814.
119 L. Wang, G. R. Li, Q. Zhao and X. P. Gao, *Energy Storage Mater.*, 2017, **7**, 40–47.
120 S. Zhao, M. Li, X. Wu, S. H. Yu, W. Zhang, J. Luo, J. Wang, Y. Geng, Q. Gou and K. Sun, *Mater. Today Adv.*, 2020, **6**, 100060.
121 D. Janas, M. Rdest and K. K. K. Koziol, *Mater. Des.*, 2017, **121**, 119–125.
122 H. Zhang, J. Xiao, J. Shi, H. Su, Y. Luo, D. Li, H. Wu, Y. B. Cheng and Q. Meng, *Adv. Funct. Mater.*, 2018, **28**, 1802985.
123 Y. Yang, M. T. Hoang, D. Yao, N. D. Pham, V. T. Tiong, X. Wang, W. Sun and H. Wang, *Sol. Energy Mater. Sol. Cells*, 2020, **210**, 110517.
124 W. Passatorntaschakorn, C. Bhoomanee, P. Ruankham, A. Gardchareon, P. Songsiriritthigul and D. Wongratanaphisan, *Energy Rep.*, 2021, **7**, 2493–2500.
125 A. A. Kuznetsov, A. F. Fonseca, R. H. Baughman and A. A. Zakhidov, *ACS Nano*, 2011, **5**, 985–993.
126 C. Peng, H. Su, J. Li, Q. Duan, Q. Li, J. Xiao, Z. Ku, J. Zhong, W. Li, Y. Peng, F. Huang and Y. B. Cheng, *Sol. Energy Mater. Sol. Cells*, 2021, **230**, 111226.
127 N. Zhang, Y. Guo, X. Yin, M. He and X. Zou, *Mater. Lett.*, 2016, **182**, 248–252.
128 F. Meng, L. Gao, Y. Yan, J. Cao, N. Wang, T. Wang and T. Ma, *Carbon*, 2019, **145**, 290–296.
129 H. Wei, J. Xiao, Y. Yang, S. Lv, J. Shi, X. Xu, J. Dong, Y. Luo, D. Li and Q. Meng, *Carbon*, 2015, **93**, 861–868.
130 P. You, Z. Liu, Q. Tai, S. Liu and F. Yan, *Adv. Mater.*, 2015, **27**, 3632–3638.
131 K. Aitola, K. Sveinbjörnsson, J. P. Correa-Baena, A. Kaskela, A. Abate, Y. Tian, E. M. J. Johansson, M. Grätzel, E. I. Kauppinen, A. Hagfeldt and G. Boschloo, *Energy Environ. Sci.*, 2016, **9**, 461–466.
132 I. Jeon, J. Yoon, U. Kim, C. Lee, R. Xiang, A. Shawky, J. Xi, J. Byeon, H. M. Lee, M. Choi, S. Maruyama and Y. Matsuo, *Adv. Energy Mater.*, 2019, **9**, 1901204–1901210.
133 K. Aitola, K. Domanski, J. P. Correa-Baena, K. Sveinbjörnsson, M. Saliba, A. Abate, M. Grätzel, E. Kauppinen, E. M. J. Johansson, W. Tress, A. Hagfeldt and G. Boschloo, *Adv. Mater.*, 2017, **29**, 1606398.
134 J. Zhang, X. Hu, H. Li, K. Ji, B. Li, X. Liu, Y. Xiang, P. Hou, C. Liu, Z. Wu, Y. Shen, S. D. Stranks, S. R. P. Silva, H. M. Cheng and W. Zhang, *Adv. Funct. Mater.*, 2021, **31**, 2104396.
135 K. M. Lee, K. S. Chen, J. R. Wu, Y. D. Lin, S. M. Yu and S. H. Chang, *Nanoscale*, 2018, **10**, 17699–17704.
136 K. K. Sears, M. Fievez, M. Gao, H. C. Weerasinghe, C. D. Easton and D. Vak, *Sol. RRL*, 2017, **1**, 1700059.
137 N. H. Khoa, Y. Tanaka, W. P. Goh and C. Jiang, *Sol. Energy*, 2020, **196**, 582–588.
138 J. J. Liang, M. Li, J. Y. Zhu, H. Zong, Y. Zhang, S. M. Jain and Z. K. Wang, *Org. Electron.*, 2019, **69**, 343–347.
139 C. Ding, L. Yin, L. Zhang, R. Huang, S. Fan, Q. Luo, J. Lin, F. Li, C. Zhao, R. Österbacka and C.-Q. Ma, *Adv. Funct. Mater.*, 2021, **31**, 2103820.
140 J. Kang, K. Han, X. Sun, L. Zhang, R. Huang, I. Ismail, Z. Wang, C. Ding, W. Zha, F. Li, Q. Luo, Y. Li, J. Lin and C. Q. Ma, *Org. Electron.*, 2020, **82**, 105714.
141 X. L. Trinh and H. C. Kim, *Energy Rep.*, 2020, **6**, 1297–1303.
142 H. Zhang, R. Liu, S. Guo, Z. Wang, X. Sun, J. Lin, Q. Luo and C. Q. Ma, *Org. Electron.*, 2022, **100**, 106352.
143 Y. Shao, Q. Wang, Q. Dong, Y. Yuan and J. Huang, *Nano Energy*, 2015, **16**, 47–53.
144 P. Li, Z. Wu, H. Hu, Y. Zhang, T. Xiao, X. Lu, Z. Ren, G. Li, Z. Wu, J. Hao, H. L. Zhang and Z. Zheng, *ACS Appl. Mater. Interfaces*, 2020, **12**, 26050–26059.
145 J. H. Heo, D. H. Shin, D. H. Song, D. H. Kim, S. J. Lee and S. H. Im, *J. Mater. Chem. A*, 2018, **6**, 8251–8258.
146 H. Spanggaard and F. C. Krebs, *Sol. Energy Mater. Sol. Cells*, 2004, **83**, 125–146.
147 R. Po, C. Carbonera, A. Bernardi, F. Tinti and N. Camaioni, *Sol. Energy Mater. Sol. Cells*, 2012, **100**, 97–114.
148 Y. Yuan, Y. Bi and J. Huang, *Appl. Phys. Lett.*, 2011, **98**, 98–100.

149 W. Gaynor, J.-Y. Lee and P. Peumans, *ACS Nano*, 2010, **4**, 30–34.
150 Y. Lu, C. Alexander, Z. Xiao, Y. Yuan, R. Zhang and J. Huang, *Nanotechnology*, 2012, **23**, 344007.
151 J.-H. Huang, Z.-Y. Ho, T.-H. Kuo, D. Kekuda, C.-W. Chu and K.-C. Ho, *J. Mater. Chem.*, 2009, **19**, 4077–4080.
152 M. Reinhard, P. Sonntag, R. Eckstein, L. Bürkert, A. Bauer, B. Dimmler, U. Lemmer and A. Colsmann, *Appl. Phys. Lett.*, 2013, **103**, 143904.
153 Y. Zhou, T. M. Khan, J. C. Liu, C. Fuentes-Hernandez, J. W. Shim, E. Najafabadi, J. P. Youngblood, R. J. Moon and B. Kippelen, *Org. Electron.*, 2014, **15**, 661–666.
154 Y. Zhou, C. Fuentes-Hernandez, T. M. Khan, J. C. Liu, J. Hsu, J. W. Shim, A. Dindar, J. P. Youngblood, R. J. Moon and B. Kippelen, *Sci. Rep.*, 2013, **3**, 24–26.
155 D. J. Lipomi, J. A. Lee, M. Vosgueritchian, B. C.-K. C. K. Tee, J. A. Bolander and Z. Bao, *Chem. Mater.*, 2012, **24**, 373–382.
156 B. A. Bailey, M. O. Reese, D. C. Olson, S. E. Shaheen and N. Kopidakis, *Org. Electron.*, 2011, **12**, 108–112.
157 W. Song, X. Fan, B. Xu, F. Yan, H. Cui, Q. Wei, R. Peng, L. Hong, J. Huang and Z. Ge, *Adv. Mater.*, 2018, **30**, 1800075.
158 Y. Wang, B. Jia, F. Qin, Y. Wu, W. Meng, S. Dai, Y. Zhou and X. Zhan, *Polymer*, 2016, **107**, 108–112.
159 J. Tong, S. Xiong, Z. Li, F. Jiang, L. Mao, W. Meng and Y. Zhou, *Appl. Phys. Lett.*, 2015, **106**, 053306.
160 M. Makha, P. Testa, S. B. Anantharaman, J. Heier, S. Jenatsch, N. Leclaire, J. N. Tisserant, A. C. Véron, L. Wang, F. Nüesch and R. Hany, *Sci. Technol. Adv. Mater.*, 2017, **18**, 68–75.
161 Z. Li, Y. Liang, Z. Zhong, J. Qian, G. Liang, K. Zhao, H. Shi, S. Zhong, Y. Yin and W. Tian, *Synth. Met.*, 2015, **210**, 363–366.
162 Z. Hu, J. Zhang and Y. Zhu, *Renewable Energy*, 2014, **62**, 100–105.
163 X. Fan, B. Xu, S. Liu, C. Cui, J. Wang and F. Yan, *ACS Appl. Mater. Interfaces*, 2016, **8**, 14029–14036.
164 H. Kinoshita, I. Jeon, M. Maruyama, K. Kawahara, Y. Terao, D. Ding, R. Matsumoto, Y. Matsuo, S. Okada and H. Ago, *Adv. Mater.*, 2017, **29**, 1702141.
165 J. J. Shen, *Synth. Met.*, 2021, **271**, 116582.
166 M. Rdest and D. Janas, *Energies*, 2021, **14**, 1890.
167 I. Jeon, C. Delacou, A. Kaskela, E. I. Kauppinen, S. Maruyama and Y. Matsuo, *Sci. Rep.*, 2016, **6**, 31348.
168 Y. H. Kim, L. Müller-Meskamp, A. A. A. A. A. Zakhidov, C. Sachse, J. Meiss, J. Bikova, A. Cook, A. A. A. A. A. Zakhidov and K. Leo, *Sol. Energy Mater. Sol. Cells*, 2012, **96**, 244–250.
169 J. Plutnar, M. Pumera and Z. Sofer, *J. Mater. Chem. C*, 2018, **6**, 6082–6101.
170 L. La Notte, P. Cataldi, L. Ceseracciu, I. S. Bayer, A. Athanassiou, S. Marras, E. Villari, F. Brunetti and A. Reale, *Mater. Today Energy*, 2018, **7**, 105–112.
171 Y. Song, S. Chang, S. Gradecak and J. Kong, *Adv. Energy Mater.*, 2016, **6**, 1600847.
172 M. M. Tavakoli, G. Azzellino, M. Hempel, A. Y. Lu, F. J. Martin-Martinez, J. Zhao, J. Yeo, T. Palacios, M. J. Buehler and J. Kong, *Adv. Funct. Mater.*, 2020, **30**, 2001924.
173 M. Nakamura, C. Yang, K. Tajima and K. Hashimoto, *Sol. Energy Mater. Sol. Cells*, 2009, **93**, 1681–1684.
174 N. Razali, I. Osaka, K. Takimiya, V. Vohra and H. Murata, *Appl. Phys. Express*, 2014, **7**, 111602.
175 F. C. Krebs, *Org. Electron.*, 2009, **10**, 761–768.
176 Z. Hu, J. Wang, X. Ma, J. Gao, C. Xu, K. Yang, Z. Wang, J. Zhang and F. Zhang, *Nano Energy*, 2020, **78**, 105376.
177 F. C. Krebs, J. Alstrup, H. Spanggaard, K. Larsen and E. Kold, *Sol. Energy Mater. Sol. Cells*, 2004, **83**, 293–300.
178 J. Y. Lee, S. T. Connor, Y. Cui and P. Peumans, *Nano Lett.*, 2010, **10**, 1276–1279.
179 R. Zhu, C. H. Chung, K. C. Cha, W. Yang, Y. B. Zheng, H. Zhou, T. Bin Song, C. C. Chen, P. S. Weiss, G. Li and Y. Yang, *ACS Nano*, 2011, **5**, 9877–9882.
180 C. C. Chen, L. Dou, R. Zhu, C. H. Chung, T. Bin Song, Y. B. Zheng, S. Hawks, G. Li, P. S. Weiss and Y. Yang, *ACS Nano*, 2012, **6**, 7185–7190.
181 A. Sharma, M. Ionescu, G. G. Andersson and D. A. Lewis, *Sol. Energy Mater. Sol. Cells*, 2013, **115**, 64–70.
182 A. R. B. M. Yusoff, S. J. Lee, F. K. Shneider, W. J. Da Silva and J. Jang, *Adv. Energy Mater.*, 2014, **4**, 1301989.
183 J. H. Lee, Y. Y. Kim and O. O. Park, *J. Mater. Chem. C*, 2018, **6**, 4106–4113.
184 J. Chae, H. Kim, S. M. Youn, C. Jeong, E. M. Han, C. Yun and M. H. Kang, *Org. Electron.*, 2021, **89**, 106046.